Universidade de São Paulo
Instituto de Geociências

Seções Balanceadas e Análise de Deformação Finita no Supergrupo Espinhaço, Porção Ocidental da Chapada Diamantina, BA.

Trabalho de Conclusão de Curso
Número TF: 21/40

Aluno: Raulindo Santana Silva Neto
NºUSP 9811769
raulindo.neto@usp.br

Orientador: Dr. Ginaldo Ademar da Cruz Campanha
Departamento de Mineralogia e Geotectônica
Instituto de Geociências

São Paulo
2022

Afastem-se, vacas, que a vida é curta!
Gabriel García Márquez
Cem anos de Solidão

Agradecimentos

Deixei para escrever os agradecimentos nos últimos dias antes da entrega desse trabalho e muito pensei sobre o que agradeceria nesse momento da minha vida. Evidentemente, extensos agradecimentos vão à minha família, em especial para minha mãe, Mary Tatiane e minha avó materna, Dona Margareth. A elas, devo carinho, amor e apoio ao longo de 6 anos de graduação, sempre querendo ter a certeza de que eu estava me alimentando bem, longe da minha saudosa terra da Bahia. Na minha família, estendo meus agradecimentos à Gel, Tia Tina, João Francisco, irmãos, primas, primos e todos aqueles que participam na minha construção como ser humano. Em especial, um grande beijo para meu irmão Arthur Veloso Lantyer!

À Kayleigh, minha companheira, obrigado pelo carinho, novas visões de mundo e por me ajudar a me tornar um homem cada vez melhor. Obrigado por compartilhar seu tempo e me permitir ser eu mesmo junto a ti. Claro, obrigado por criar as mais lindas gatas, Dona Márcia e Joana Maria.

Muito tenho a agradecer ao Professor Ginaldo Campanha que me orientou durante a graduação desde 2018, quando iniciamos o projeto base desse Trabalho de Formatura, como Iniciação Científica. Muito obrigado pela disposição e cooperação durante o desenvolvimento do trabalho, bem como o esforço para fazer acontecer o estágio de pesquisa no exterior.

Aproveito para agradecer aos Drs. Oskar Vidal-Royo, Alejandro Amilibia-Cabeza e Hodei Uzkeda pelo suporte durante minha estadia em Barcelona para o desenvolvimento de parte desse Trabalho de Formatura. Essa colaboração foi essencial para o progresso do trabalho. ¡Muchas gracias, chicos!

Aos meus professores Mário Campos, Renato Paes de Almeida, André Sawakuchi, Frederico Faleiros e Claudio Mora. Ao longo de tantas horas de aulas, tive o privilégio de aprender Geologia com vocês, além de me atentar cada vez mais para a importância da educação.

Aos colegas e amigos de GEO, João Zwarg, Teyzinha, Chokany, Marginaldo, Singanô, Sid, Nesquik, Iludida, Carniça, e todos mais, pelos incontáveis momentos de convivência e partilha durante a graduação, nos campos, nos ônibus até os campos, na realidade paralela da sala 108 e no bandeco. Ao time de vôlei da GEO, Lelek, Piriguete, Pika, Bug, Arregão, Jaque, Pedrita e Sheilla, pelos BIFEs e os raros, porém memoráveis, momentos vitoriosos.

Aos meus eternos amigos de Feira de Santana, Caio Figueiredo, Clébio Júnior, Matheus Morais e Valmiro Neto, pelos momentos de descontração e risadas!

À FAPESP, pelo apoio financeiro, sob o projeto n^o: 2020/03337-0 e pela bolsa CNPq-PIBIC (Proc. 144943/2018-2).

Por fim, mas não menos importante, um agradecimento especial para todos os trabalhadores e servidores do Instituto de Geociências, da Universidade de São Paulo e do CEPE - faxineiros(as), porteiros(as), seguranças, motoristas e cozinheiros(as) dos restaurantes universitários. A USP não seria nada sem o trabalho de vocês!

ABSTRACT

The Paramirim aulacogen is understood as an intracontinental rift system, nucleated around 1.75 Ga, in the central region of the São Francisco craton (CSF), which enabled the deposition of thick sedimentary sequences, predominantly siliciclastic, such as the Espinhaço and São Francisco supergroups. The complex tectonic evolution of the CSF involves, recently, an intense process of collisions and docking during the Brasiliano cycle around 640-500 Ma, which culminated in the formation of the western Gondwana megacontinent. In this context of tectonic inversion, the Paramirim aulacogen developed important shear zones and intracratonic thrust and fold belts. Despite the intense study regarding the tectonic evolution of the area, little is known in quantitative terms about the geometry, kinematics, magnitude and mechanisms of the deformation involved in the aforementioned geological event. In this study, strain magnitude and tectonic shortening across the Western Chapada Diamantina fold-and-thrust belt are calculated by finite strain analysis using mainly detrital quartz grains as strain markers and by cross-section restoration and forward models. A total of 9 complete 3D strain analyses on oriented samples were conducted by the Inertia Tensor method and best fit ellipsoids were computed, resulting in strain ratios (X/Z) varying from 1.190 to 2.504. Predominant oblate shaped ellipsoids related to down-dipping stretching directions are associated with regional transport direction from SW to NE, with reverse faults, upright axial-plane fold and sub-horizontal axis. The restoration of the cross-section yielded a shortening of 19.37%, understood as the minimum tectonic shortening associated displacement associated with faults, bed rotation and the ductile strain flattening related with the unfolding. The proposed model is consistent with the geometry relationship between the former rift architecture controlling the folding style affecting the sedimentary cover, where the reactivation of normal faults rules the localization and kinematics of thrust ramps, with basement involvement in a thick-skinned tectonic style. Similarly, the assessment of the forward models resulted in a minimum shortening of 18.5%. Comparably, finite strain data integration techniques yielded a total of 21.65% of regional tectonic shortening, representing the horizontal component of ductile flattening strain across the section due to penetrative strain. Therefore, we present, by three different and independent approaches, an estimate range of tectonic shortening between 18-22% at the western Chapada Diamantina region, but the total amount of shortening across the Paramirim aulacogen might have been greater. These results suggest that the western and eastern parts of the São Francisco craton could not be considered as rigidly linked during the Neoproterozoic - Cambrian Brasiliano orogeny being separated by the Paramirim aulacogen.

RESUMO

O aulacógeno do Paramirim é entendido como um sistema de riftes intracontinentais, nucleado em torno de 1,75 Ga, na região central do cráton do São Francisco (CSF) que possibilitou a deposição de espessas sequências sedimentares, predominantemente siliciclásticas, como os supergrupos Espinhaço e São Francisco. A complexa evolução tectônica do CSF envolveu um intenso processo de colisões e docagens durante o ciclo Brasiliano em torno de 640-500 Ma, que culminou na formação do megacontinente Gondwana ocidental. Nesse contexto de inversão tectônica, o aulacógeno do Paramirim desenvolveu importantes zonas de cisalhamento e cinturões de empurrão e dobramento intracratônicos. Apesar do intenso estudo a respeito da evolução geotectônica da área, pouco se sabe, em termos quantitativos e práticos, à respeito da geometria, cinemática, magnitude e mecanismos da deformação envolvidas no evento geológico supracitado. Neste estudo, a magnitude da deformação e o encurtamento tectônico ao longo do cinturão de empurrão e dobramento Chapada Diamantina Ocidental são, respectivamente, calculados por análise de deformação finita usando grãos de quartzo como marcadores de deformação e estimados por restauração de seção geológica e *forward models*. Um total de 9 análises de deformação 3D completas em amostras orientadas foram conduzidas pelo método do Tensor de Inércia e os elipsóides de melhor ajuste foram calculados, resultando em razões de deformação (X/Z) variando de 1,190 a 2,504. Elipsóides de formato oblato estão relacionados às direções de alongamento de mergulho *down-dip* e associados à direção de transporte regional de SW para NE, com falhas reversas, plano axial vertical em dobras e eixo sub-horizontal. A restauração da seção geológica resultou um encurtamento de 19,37%, entendido como o encurtamento tectônico mínimo associado ao deslocamento associado às falhas, à rotação de camadas e à deformação dúctil relacionada ao desdobramento. O modelo proposto é consistente com a relação geométrica entre a antiga arquitetura inicial do rifte controlando o estilo de dobramento que afeta a cobertura sedimentar, onde a reativação das falhas normais rege a localização e cinemática das falhas de empurrão no estilo tectônico *thick-skinned*. Da mesma forma, a avaliação dos modelos *forward* resultou em um encurtamento mínimo de 18,5%. Comparativamente, as técnicas de integração de dados de deformação finita resultaram um total de 21,65% de encurtamento tectônico regional, representando o componente horizontal da deformação de dúctil em toda a seção devido à deformação penetrativa. Portanto, apresentamos, por três abordagens diferentes e independentes, um intervalo estimado de encurtamento tectônico entre 18-22% na porção ocidental da Chapada Diamantina, porém a quantidade total de encurtamento em todo o aulacógeno do Paramirim pode ter sido muito maior. Estes resultados sugerem que as partes ocidentais e orientais do cráton do São Francisco não podem ser consideradas como rigidamente ligadas durante a ciclo Brasiliano sendo separadas pelo aulacógeno do Paramirim.

CONTENTS

1 INTRODUCTION

The Paramirim aulacogen or corridor is understood as an intracontinental rift system nucleated in the Statherian Period in the central area of the São Francisco-Congo craton, which provided an accommodation space for a long bacinal stage with alternating pulses of mechanical and flexural subsidence (Pedrosa-Soares and Alkmim, 2011; Cruz and Alkmim, 2017). The filling units are mainly siliciclastic and metavolcanic rocks of the Espinhaço Supergroup that outcrop in the Northern Espinhaço range toward west, in the Paramirim valley in the central region and in Chapada Diamantina in the eastern region (Fig. 1)(Danderfer Filho, 1990; Danderfer and Dardenne, 2002; Guimarães et al., 2008; Cruz and Alkmim, 2017).

During the Brasiliano-Pan African orogenic cycle (Ediacaran period), the Paramirim aulacogen was partially inverted due to the amalgamation of Western Gondwana paleocontinent. During this context of tectonic inversion, two thrust-and-fold belts were developed, Northern Espinhaço range and Chapada Diamantina, with thick and thin skinned deformation. Thus, the dominant model suggests that the Paramirim aulacogen is an inverted rift, where the normal faults were reactivated as thrust faults, encompassing the Neoproterozoic deformation and the fold-and-thrust belts crossing the central portion of the craton (Cruz and Alkmim, 2006; Cruz et al., 2015; Cruz and Alkmim, 2017; Danderfer and Dardenne, 2002; Guimarães et al., 2008; Danderfer Filho, 1990).

Although the model of an indivisible São Francisco craton, as proposed by Almeida (1977), has been predominant in the regional literature, another models have already been proposed, as the existence of two cratons, São Francisco and Salvador, separated by the Paramirim aulacogen (Cordani, 1973*a*,*b*, 1978; Trompette et al., 1992*b*,*a*).

Furthermore, the confined character of the Araçuai – West Congo orogen, as proposed by Pedrosa-Soares et al. (2001), due the existence of the Gabon – Salvador bridge joining the São Francisco and Congo cratons, puts geometrical and kinematic issues on the orogenic tectonic evolution, as well as in the role and displacement of the aulacogens crossing the São Francisco craton. (Cavalcante et al., 2019; Fossen et al., 2020). One of the hypotheses proposed to solve the question is the “nutcracker” model by Alkmim et al. (2006).

Processes of inversion and basement fault reactivation during the Neoproterozoic evolution can be eased by structural inheritance, which act as an important control on intracratonic deformation (Butler et al., 2006). Apart from the Paramirim aulacogen, structural inheritance is observed elsewhere within the São Francisco craton (Martins-Ferreira, 2019).

Thus, the refinement of the models currently proposed for the São Francisco craton and its associated units comprises challenges and issues still under discussion. Among these, quantitative approaches to deformation, such as 3D strain analysis, the use of forward models and restorable cross sections are scarce in Brazilian orogen-related basins, but they are no less necessary.

Quantitative strain data represent an important aspect of deformation style and kinematics in orogenic belts, and can provide hints of processes for tectonic evolution. For this region, this procedure is easily applied in low-grade metasedimentary rocks, due to the high exposure of outcrops and meta-sandstones units capable of registering deformation on single quartz grains.

On the other hand, section balancing is a classical technique to obtain and evaluate the accuracy and consistency of an interpreted geological section, where the main purpose consists of validating the structural interpretation of the proposed model and its geometry, by adding extra geometric rules that need to be followed in order to consider a section balanced (Dahlstrom, 1969). Additionally, in areas where subsurface data is scarce and the geology is complex, forward modelling is a powerful tool to test ideas and understand the processes and kinematics involved in the deformation (Mount et al., 1990).

Having said that, the main goals of this study are (i) to compute and discuss 3D strain data of best-fit ellipsoids from single detrital quartz grains as strain markers (ii) to estimate the minimum amount of tectonic shortening suffered by the Paramirim aulacogen. For these purposes, balanced cross-sections were constructed across the Chapada Diamantina Fold-and-Thrust Belt, based on surface data, forward models were created and strain analysis were carried out on rocks from the Espinhaço Supergroup. In this way, new insights were obtained to analyze the amount of displacement and deformation involved within the Paramirim aulacogen, which is the main objective of the present contribution.

2 REGIONAL GEOLOGICAL CONTEXT

The study area is located in the São Francisco craton (SFC) (Figure 1), understood as an Archean to Paleoproterozoic continental block which maintained tectonic stability during the orogenetic processes of the Neoproterozoic Brasiliano-Pan African cycle (Almeida, 1977). Due to previous residency in the Rodinia supercontinent, the SFC has its cratonic counterpart present in the African continent today, which together composed the São Francisco - Congo paleocontinent (Brito Neves et al., 1999; Almeida, 1977).

The basement of the São Francisco craton is the result of accretionary processes of Meso to Neoarchean continental fragments and it is composed essentially of medium to high grade metamorphic rocks such as orthogneisses, K-rich metagranitoids, TTG's suites and associations granite-greenstone belts, corresponding mainly to the elongated North-South segment of the craton (Teixeira et al., 2017). The main archean nucleus of the cratonic basement are the Gavião Block on the western sector and the Serrinha and Jequié blocks to the east, all of which register post and late-orogenic granite intrusions during Rhyacian and Orosirian ages (Pedreira et al., 1975; Barbosa and Sabaté, 2002, 2004; Cruz et al., 2016)

The Paramirim aulacogen, originally called the Espinhaço aulacogen (Costa and Inda, 1982), is understood as an intracontinental rift system occurring on the Gavião block, associated with the development of several sedimentary basins from the Statherian, ca. 1775 $\pm$ 75 Ma until the Tonian (ca. 850 Ma) (Cruz and Alkmim, 2006, 2017; Pedrosa-Soares and Alkmim, 2011; Danderfer and Dardenne, 2002; Danderfer et al., 2009; Alkmim et al., 2001). Crystallization ages of ca. 1750 Ma of alkaline anorogenic intrusive metagranitoids of the Lagoa Real Intrusive Suite as the volcanic suites of the Rio dos Remédios Group are interpreted as the the age of initial rifting process (Cordani et al., 1992; Turpin et al., 1988; Cruz and Alkmim, 2006; Cruz et al., 2007).

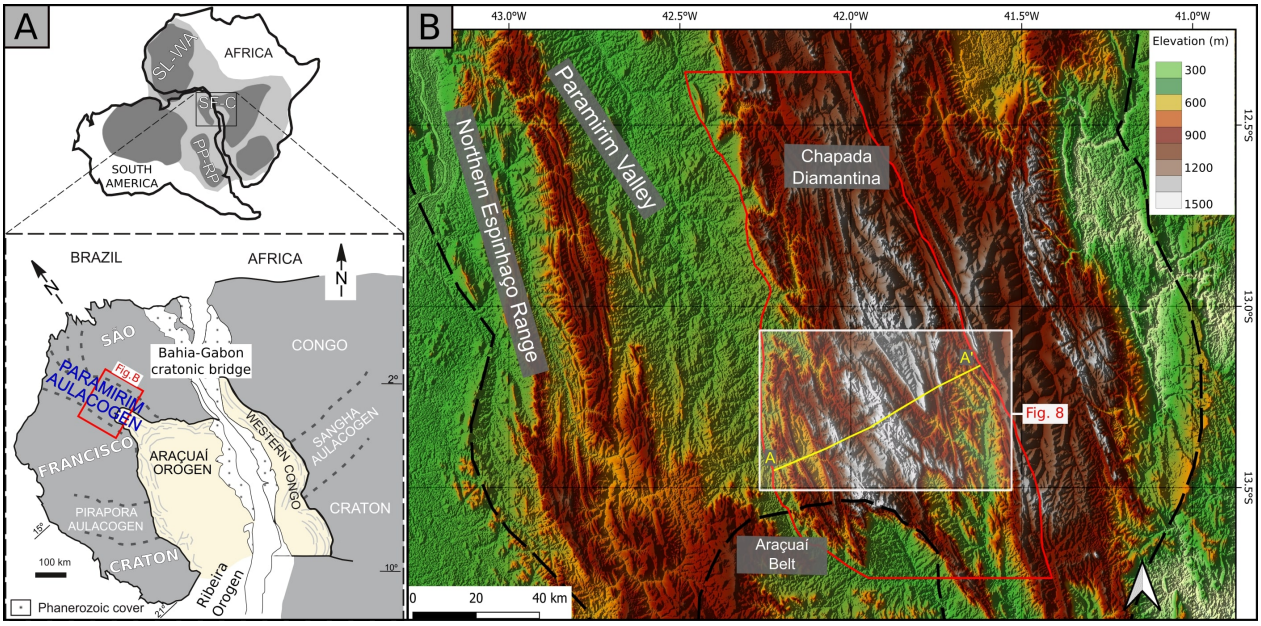

Figure 1: A: Tectonic compartment of the Paramirim aulacogen within the São Francisco-Congo craton and the adjacent Araçuaí-West Congo orogen. Modified from Pedrosa-Soares et al. (2008); **B:** The red line bounds the study area location and adjacent morphological domains. The white rectangle represents the area of Figure 8 and the yellow line is the studied cross section (A-A').

The main sedimentary filling units that cover the aulacogen's basement are the Espinhaço and São Francisco supergroups. The Espinhaço Supergroup is the main subject of this study and it is a succession of siliciclastic rocks, comprising metasandstones, metaconglomerates and metapelites, with intercalation of metavolcanic rocks. The Espinhaço Supergroup outcrops in a large area, but it is mainly recognized in the Northern Espinhaço range and Chapada Diamantina thrust-and-fold belts. In the Chapada Diamantina region (Fig. 2), the entire package is subdivided from bottom to top in the Serra da Gameleira Formation and three groups, Rio dos Remédios, Paraguaçu and the homonyms group Chapada Diamantina (Guimarães et al., 2008, 2012).

The Serra da Gameleira Formation occurs as a continuous composed predominately of aeolian sandstones, on top of the basement marked by a regional erosive and angular unconformity, interpreted as a pre-rift sedimentation phase (Guimarães et al., 2008). Petrographic analysis for this units points to clast supported sandstones, composed predominantly by fine-medium single quartz grains, with the presence of muscovite within the matrix and no contribution of lithic fragments.

The Rio dos Remédios Group comprises a succession of acid lavas and lacustrine to alluvial sedimentary units and registers mechanical and thermal subsidence events that took place at the basin during the syn-rift phase (Guimarães et al., 2008). It is subdivided into three formations: The basal Novo Horizonte Formation covers a range of volcanic and epiclastic rocks, interpreted as deposited associated with initial rifting pulses and the related magmatism. It is followed upwards by the Lagoa de Dentro Formation, grouping interbeded sandstones and pelites. Finally, at the top of the group, lies the Ouricuri do Ouro Formation, a package of conglomerates and sandstones. Both the Lagoa de Dentro and Ouricuri do Ouro formations corresponds to the continental sedimentation phase that followed the initial rifting (Guimarães et al., 2008).

The Paraguaçu Group overlaps the lower Rio dos Remédios Group by an erosional or tectonic unconformity and marks a shift from tectonic control to a passive subsidence sedimentation pattern, being commonly associated to post-rift sag sequence in a phase of basin expansion, subdivided into two formations (Cruz and Alkmim, 2017; Guimarães et al., 2008; Loureiro et al., 2009). At the base, Mangabeira Formation comprises essentially marine sandstones and pelites. The upper Açuruá Formation is composed by shallow marine sandstones and pelite (Guimarães et al., 2008).

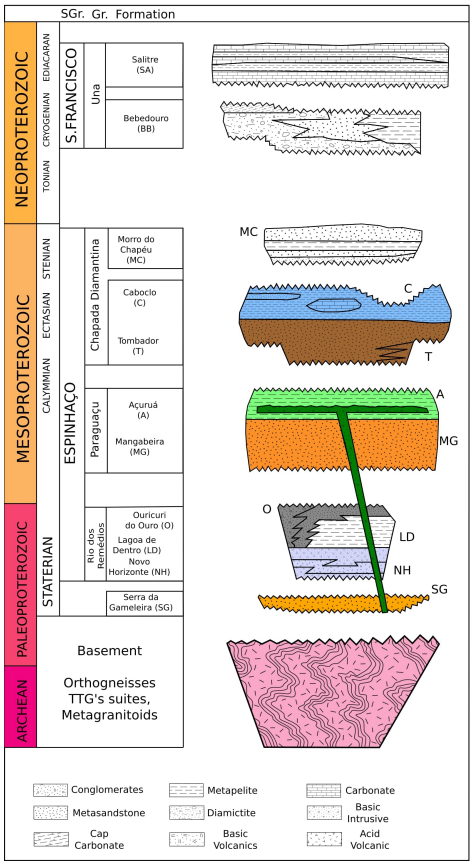

Figure 2: Stratigraphic chart of Chapada Diamantina in the Paramirim Aulacogen. Based from Alkmim and Martins-Neto (2012), modified after Cruz and Alkmim (2017). The colors match the same color code by formation of Fig. 8.

Finally, the Chapada Diamantina Group has a major North-South orientation with a sag geometry very similar to the post-rift Paraguaçu Group's, switching from marine sedimentation into continental sedimentation marked by an erosive unconformity (Guimarães et al., 2008). Only two of the three formations that compose this group outcrop at the study area. At the base, the Tombador Formation comprises a package of fluvial/shallow marine sandstones and detritical diamond bearing conglomerates that grade upward into shallow marine pelites with carbonate lenses of Caboclo Formation (Guimarães et al., 2008; Cruz and Alkmim, 2017).

Although depositional ages are well constrained by recent contributions (Guadagnin et al., 2015; Guadagnin and Chemale Jr., 2015), the sedimentary package's thickness is not, lacking a precise estimate of maximum thickness. Geological mapping surveys estimate a total thickness

around 5.700 meters, with possible major variation within the sedimentary cover (see Guimarães et al. (2008) and references therein).

During the Brasiliano-Pan African Global orogenic cycle, there were successive terrane collisions and docking that resulted in the last amalgamation of the ancient cratons, including the SFC, to form the supercontinent Gondwana, between 640 and 500 Ma (Campos Neto, 2000; Almeida et al., 2000). In this context, the tectonic inversion of the aulacogen took place under a general ENE-WSW compression, which also corresponds to the general stress field to which the craton was subjected during the collisional event (Cruz and Alkmim, 2006; Cruz et al., 2015).

The overall structural framework of the Paramirim Aulacogen consists of two main fabric elements associated to original extensional processes related to rifting and contractional structures associated to the inversion of the basin (Danderfer Filho, 1990; Cruz and Alkmim, 2006; Cruz et al., 2015). Field data and map interpretation indicate that pre-existing normal faults can be considered as mechanical anisotropies planes, effectively controlling localization and kinematics of thrust ramps and are related to fold nucleation on the sedimentary cover (Martins-Ferreira, 2019).

3 MATERIAL AND METHODS

3.1 Database

The used database consisted of field data and oriented samples collected along a section nearly orthogonal to the regional structures, as well as published and unpublished archival and open-access structural data from geological mapping, from the Geological Survey Company of State of Bahia (Companhia Baiana de Pesquisa Mineral - CBPM). Surface geometries are based on 1:200.000 scale syntheses geological maps of the Paramirim aulacogen and also on Digital Terrain Model obtained from 30 m resolution SRTM images (USGS/NASA). Once there are not any seismic lines and/or borehole within the study area, the subsurface interpretation is constrained only by surface geometry and lithological relationships.

3.2 Finite Strain Analysis

Oriented samples for strain analysis were collected along the section trace, focusing specially on quartz grains-supported sandstones and siltstones units. For each sample, 2D shape preferred orientation (SPO) analysis were carried out on roughly orthogonal planes, using the methodology described by Launeau and Cruden (1998). With the mean ellipse adjusted for each plane, a 3D best-fit ellipsoid was then fitted for each sample and used to calculate the 3D finite strain ellipsoid. The finite strain analysis workflow is summarized in Figure 3.

3.2.1 Sample Preparation

Cut planes for 2D strain analysis were made for each sample and measured with its orientation (strike/dip) annotated using the RHR rule (Fig. 3A). The planes need not to be necessarily perpendicular, although further calculation is optimized when high angles (approximately 90°) are included (Ramsay, 1967; Robin, 2002).

Two photomicrographs were taken and used to draw quartz grains using the Illustrator vector graphical editor software (Figs. 3B-C) from which the Shape Preferred Orientation (SPO) was obtained by the Inertia Tensor method (Robin, 2002; Launeau and Cruden, 1998).

3.2.2 2D Strain Measurement

Shape Preferred Orientation method was applied to the prepared samples to automatically generate best-fit ellipses of clasts and produce measurement-orientation of the shape ratio (Sr) and long-axis orientation (ϕ) of each grain (Launeau and Cruden, 1998). At least 80 clasts for each plane were analyzed and the results were used to calculate the Mean Shape Preferred Orientation of the 2D section and its aspect ratios, Sr and ϕ, by stacking all individual SPO of the grain population on their gravity center (Figs. 3D-E).

Because of the erasing of all grains cut by the image border required by the inertia tensor method, a test of invariance by translation is setup to proof that 2D SPO are unbiased (Launeau and Robin, 2005). To do so, in this study, a subset window set to a $\frac{3}{4}$ of the image is translated on 4 positions with an overlapping of 50% between each other's allowing the calculation of 4 subset SPO per image (Fig. 3E). A simple standard deviation between subset SPO for all parameters allows the evaluation of the homogeneity of the data throughout the full image and will attest of their unbiased quality. Similar analysis with subsets is commonly used in mathematical morphology (Serra, 1982). All results of SPO analysis are reported in the Appendix.

One must bear in mind that the computed tensor solely describes the shape of the object and do not necessarily correspond to the finite strain ellipsoid. However, for deformed objects whose initial geometry is approximately equidimensional tending to spherical or elliptical shapes, such as quartz grains, and there is no viscosity contrast between the clast and the matrix, the strain and shape ellipsoid can be assumed as equal (Launeau and Robin, 2005,?; Faleiros, 2008).

3.2.3 3D Strain Best Ellipsoid Fitting

Based on the sectional ellipse data from arbitrary non parallel planes AC, AB and BC for each sample, the measurement-orientation parameters, such as the shape ratio (S_r), inclination and planar orientation, were used to calculate a best-fit 3D ellipsoid using the software *ELLIPSOID* (Robin, 2002; Launeau and Robin, 2005). This method consists of an algebraic solution, where sectional data for each sample can build a system of linear equations used to compute the six unknown coefficients that describe the ellipsoid (Robin, 2002).

The program *ELLIPSOID* also quantifies the difference between measured ellipses of any faces, a scalar parameter called "incompatibility index" ($\sqrt{\tilde{F}}$) from a section of the best-fit resulting ellipsoid (Robin, 2002). The 2D SPO test of invariance by translation giving 4 subset SPO per image section their combination results in 64 (4^3) subsets of 3D ellipsoids for every outcrop (Fig. 3F) (Launeau and Robin, 2005). Having around 80 grains per section combined by roughly 3 times 60 (180) grains per subset ellipsoid ($N \approx N - 1$) we may consider 2σ as an estimation of a 95% confidence interval for all parameters.

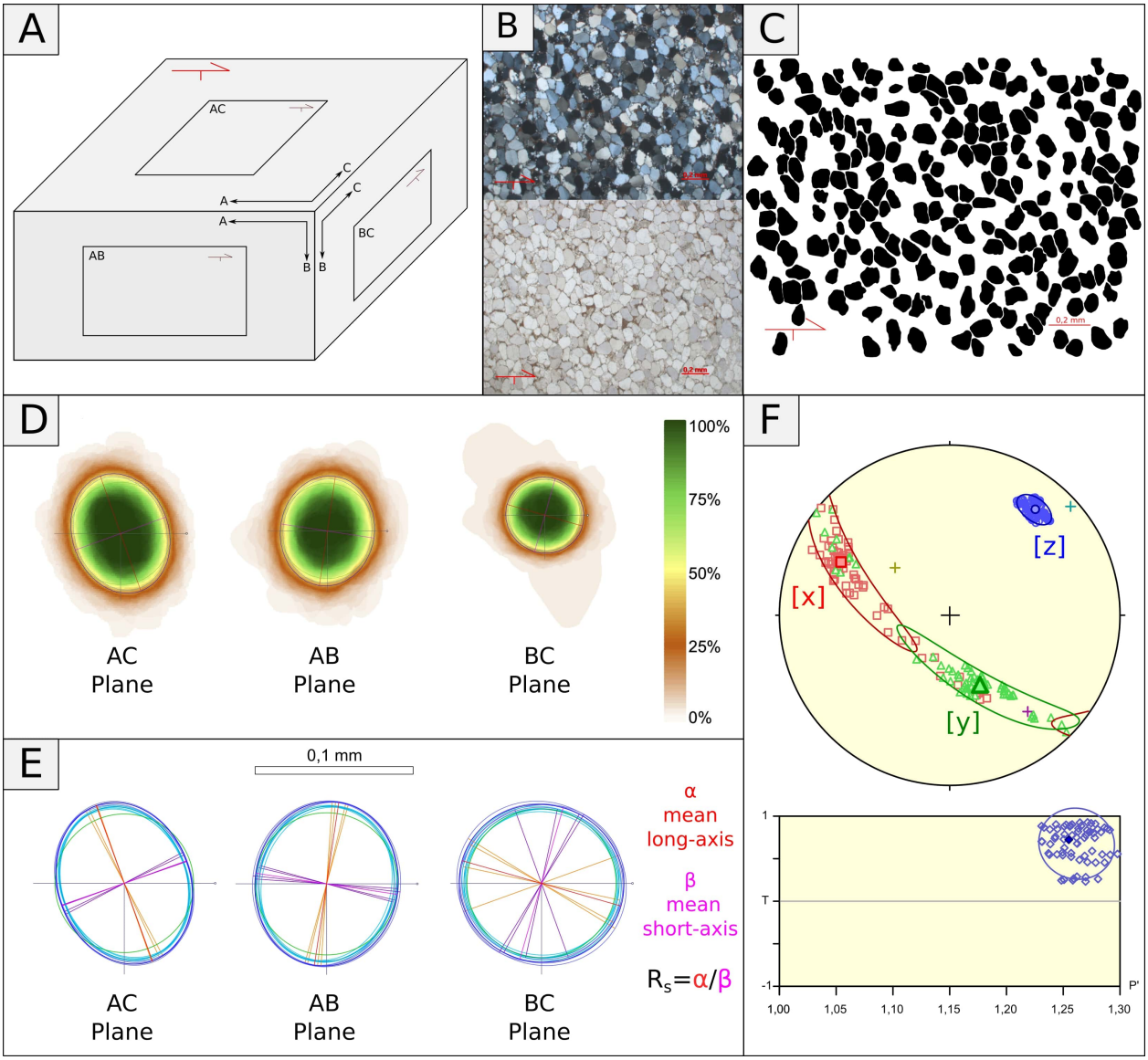

Figure 3: (A): Block diagram representing general orientations of AC, AB and BC thin-section cut planes for each sample; **(B):** Oriented thin-section photomicrograph of sample CD-30A; **(C):** Raster image containing single quartz grains digitized from thin-sections photomicrographs of sample CD-30A.; **(D)**: Once all images from each sample were processed through steps B and C, the Mean Shape Preferred Orientation (SPO) for each plane was analysed. The Shape Ellipse can be understood as the strain ellipse acting on the given plane (see text); **(E):** SPO ellipses calculated by the test of invariance by translation, and its measurement and orientation parameters, such as long-axis (α), short-axis (β) and the shape ratio Rs; **(F)**: 64 subset ellipsoids produced for sample CD-30A, with 2σ confidence interval around each axial pole. All the result parameters for the ellipsoid are reported in Table 1 and in the Appendix.

3.3 Balanced Cross Sections and Forward Models

Balancing (Dahlstrom, 1969) can be defined as a set of geometric rules applied to geological cross sections to validate the kinematical and geometrical viability of the proposed model. This method is usually applied to quantify deformation, reverse the process of strain as a mode to illustrate geologic evolution through time and reduce geological uncertainty in deep subsurface.

Balancing a cross section requires mass conservation before and after deformation, as in a balance (Figure 4). A further common constraint in contractional settings is conservation of bed length of stratigraphic units before and after deformation (line length validation). The construction, balancing and restoration of the geological cross sections area a powerful method to analyze and quantify the deformation of an area, while also validating structural interpretations, calculating minimum tectonic shortening and assessing subsurface crustal structures presents in the model (Dahlstrom, 1969; Elliott, 1983).

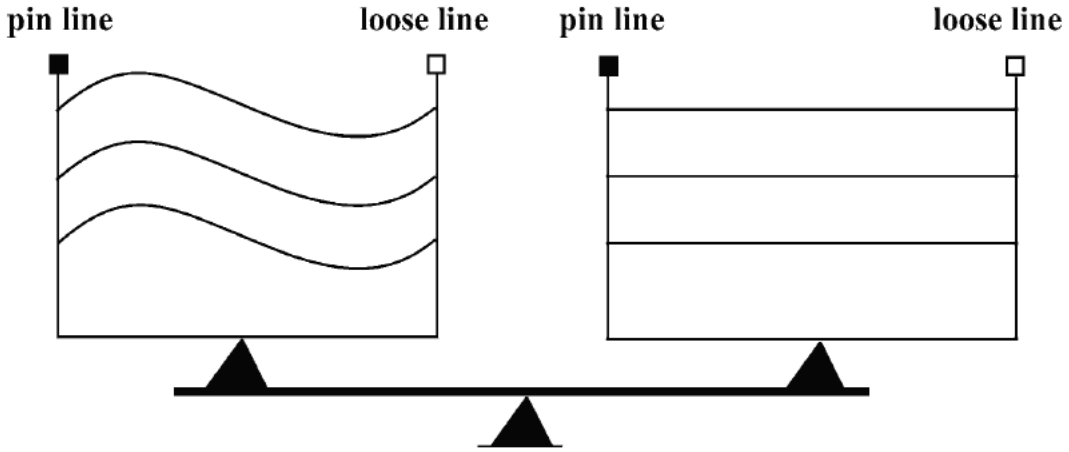

Figure 4: The concept of a balanced geological cross section with area (mass and length) conservation in the pre-deformation state and deformed state (Groshong Jr, 2006).

There are four principles that a geologic model must meet to be considered as balanced (Dahlstrom, 1969; Elliott, 1983; Vidal-Royo et al., 2015):

i) **Accuracy:** it must fit the available data constraints;

ii) **Admissibility:** it must conform to structural geometries recognized in local or analogous areas, usually natural, but sometimes experimental or theoretical;

iii) **Restorability:** it can be returned to a pre-deformational geometry, in a single step or in multiple steps;

iv) **Balance:** the restoration must display balanced bed lengths and/or areas, among others.

The field of Structural Geology is often concerned about the errors involved in the construction of cross sections, where the initial stratigraphic settings are the primary source of error for further

interpretations (Judge and Allmendinger, 2011). In areas with limited subsurface data, forward modelling is a useful method which can provide insights regarding the style and kinematical evolution of structures during deformation (Mount et al., 1990). Forward modelling is a technique that simulates, from geological information, the evolution of a model in order to replicate a synthetic outcome that matches actual observations.

We conduct the construction of forward models to approximate the observed regional structures, respecting dip data, dimension of structural and overall main geometry, following the fault-related fold theory (Suppe, 1983). Repeatedly modelling was necessary to estimate the parameters that best visual fit the original data and interpretation to reach a closer match.

Forward models and balanced cross sections were constructed using the 2D kinematic modelling algorithms implemented in the Petex MOVE® software. For forward modelling the Simple Shear algorithm was used for both normal faulting during extension phase and thrusting, during tectonic inversion. The Trishear algorithm was also used during the inversion to generate fault-propagation folds. The algorithms used might trigger minor thickness variations close to the hanging walls, but it doesn't affect the overall regional geometry of the model. The cross-section restoration used the bed-length method, which models deformation by flexural slip, which maintains bed thickness.

3.4 Strain Integration

The strain integration technique is described by Woodward et al. (1986), which computes the undeformed length of a strain trajectory by a simple integration of the reciprocal stretch along the trajectory in the current deformed state. This method can be used to estimate the regional strain and the amount of shortening due to penetrative strain (Hossack, 1978).

Once the ellipsoids are adjusted and the stretches are calculated for each locality, the reciprocal stretch, represented by $1/S$, where stretch (S) is defined as the ratio between the final and the initial length of a line, is plotted versus the distance along the section. The area under the curve is equivalent to original length (L_o):

$$L_o = \int \frac{1}{S}\, dl \tag{1}$$

Then the original length (L_o) and the current deformed length (L) gives the percentage of shortening in the section represented by its elongation (e).

$$e = \frac{L - L_o}{L_o} * 100 \tag{2}$$

4 RESULTS

4.1 The Studied Area

A field section was carried out from the localities of Caraguataí, Piatã, Inúbia, Érico Cardoso and Paramirim (Bahia State) trying to be as orthogonal as possible to the regional geological structures (Fig. 8). It encompass the main lithostragraphic units of the Western Chapada Diamantina region, including the Archean basement represented by the Gavião and Paramirim complexes as well granitic rocks, and the Statherian to Stenian low-grade metasedimentary and metavolcanic units of the Espinhaço Supergroup (see Fig. 8).

The region is characterized by open to gentle regional folds with hectometric to kilometric wavelength and decametric to hectometric amplitudes, as well by steep reverse faults. The Archean basement and the basal Rio dos Remédios Group occupy the cores of the major anticlines, and the upper Paraguaçu and Chapada Diamantina groups the cores of main synclines. The different lithostratigraphic units usually show a strong geomorphological contrast, specially the Tombador Formation of the Chapada Diamantina Group , allowing to perceive the main structural framework in the topography and digital terrane models, easing the contact tracing.

The Archean basement outcrops in the Teixeira range, next to the cities of Caraguataí and Abaíra, as well in the westernmost portion of the studied area, where the Archean Paramirim Complex is thrusted over the Espinhaço Supergroup. The upper Paraguaçu and Chapada Diamantina groups outcrop mainly in the Piatã and Érico Cardoso synclines.

As the rocks of the Espinhaço Supergroup are affected by very low grade metamorphism (low greenschist facies), the primary structures in metasedimentary and metavolcanic rocks are abundant, as well preserved plane-parallel bedding, cross-stratification, ripple marks and conglomeratic beds. A fine slaty cleavage is developed characterized by the alignment of fine sericite and elongation of clastic grains, pebbles, volcanic amygdules and tuffs. The slaty cleavage usually cross cuts the sedimentary bedding at moderate to high angles, except near shear zones and faults, where a parallelism between bedding and tectonic cleavage is observed. The metasandstones and metapelites in thin-section generally feature visible primary structures, with very low grade metamorphism. They show sub-rounded to rounded clastic texture and are moderately sorted, being dominantly composed by single quartz grains (Fig. 6D-E). Kinematic indicators in the collected samples show mainly an overall sense of transport to northeast (Fig. 6F). On the other hand, the basement rocks are affected by much higher grade of metamorphism (medium to high amphibolite) with isoclinal folding and transposition of gneissic bands and leucossomes, with strong foliation and stretching lineation.

Orientation data compiled from Guimarães et al. (2008) and our field collected data are shown in stereograms (Fig. 5). Figure 5A shows the primary bedding poles delineating a great circle girdle denoting the open to gentle folding, with a mean sub-horizontal NE fold axis and two clusters with moderate dips to NE and SW, reflecting the fold limbs. Calculated $\pi - pole$ of 334/03 (trend/plunge) coincides with the clustering of intersection lineation data, interpreted as the main fold axis orientation. Figure 5B shows the tectonic foliation poles with a cluster indicating a mean

upright attitude with NE strike and strong dip to SW. Figure 5C shows the stretching lineation with mean down-dipping attitudes regarding the tectonic foliation. The attitude data and kinematic indicators corroborate the regional transport direction from SW to NE, associated with reverse faults, fold upright axial-plane and sub-horizontal axis.

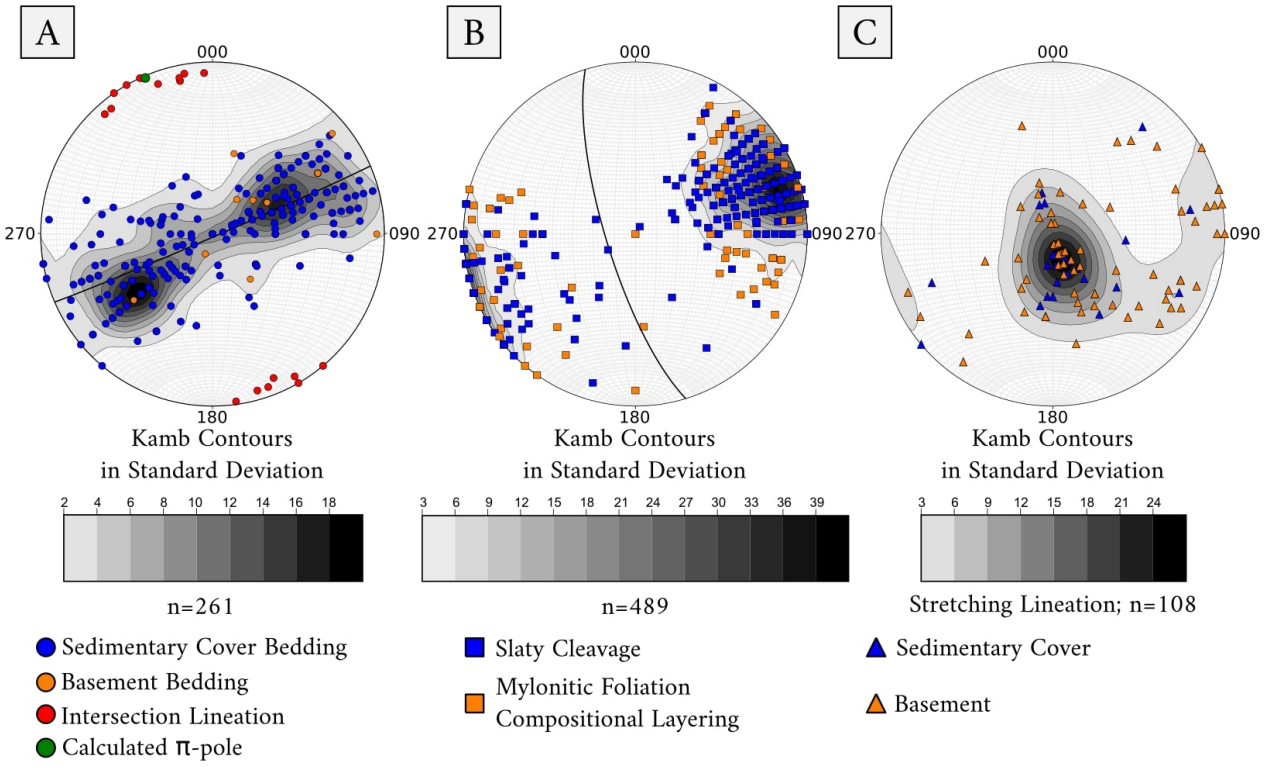

Figure 5: Stereogram (lower hemisphere, equal area projections) presenting structural data collected by 1:200.000 scale geological mapping (Guimarães et al., 2008) and our field work.

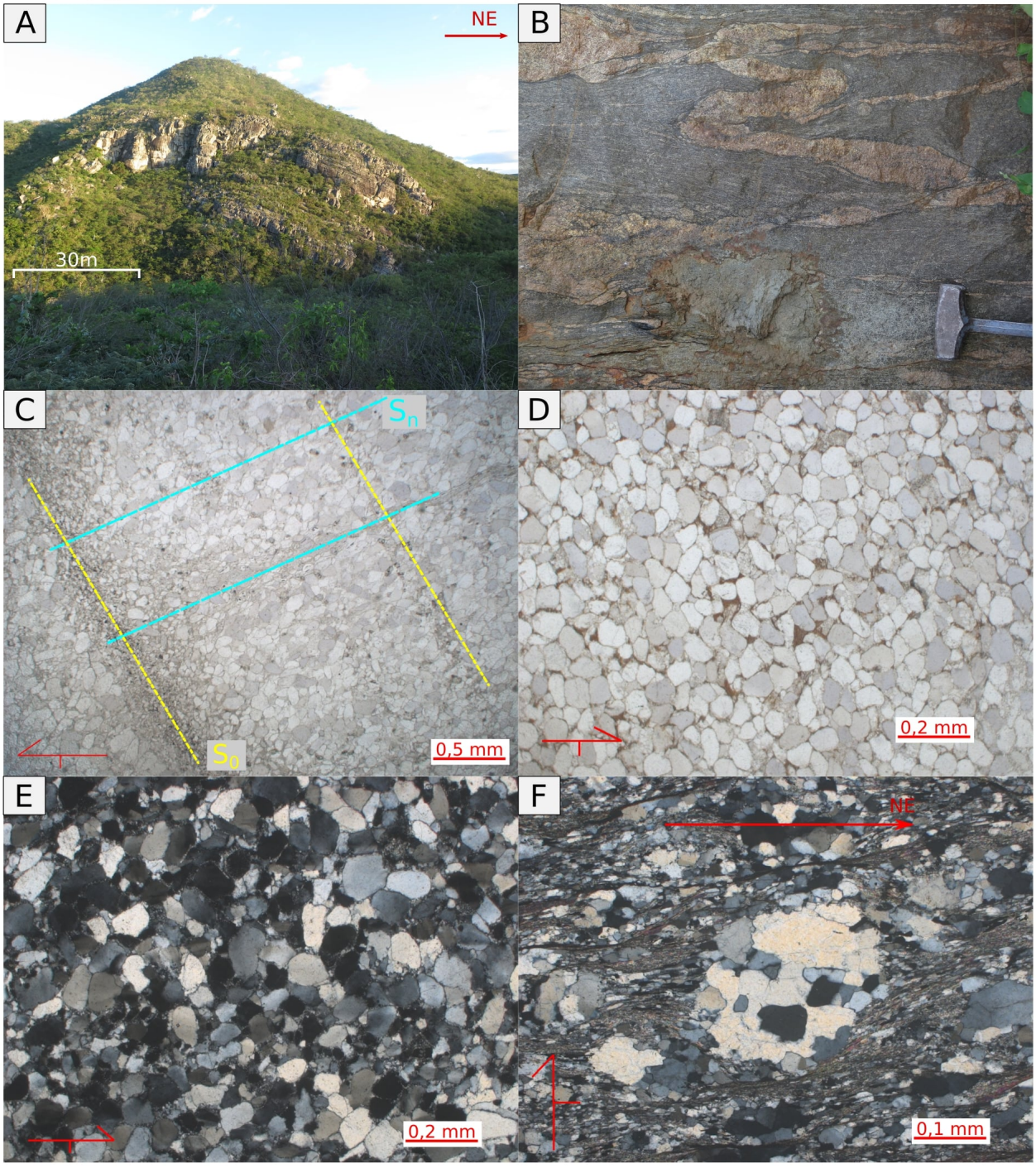

Figure 6: Geological micro- and macro-structures from the study area. **A)** Mesoscopic scale fold from the upper beds of Paraguaçu Group, showing very gentle folding pattern. **B)** Deformed orthogneiss with isoclinal folding afecting pegmatitic leucossomes with a plane-axial schistosity. **C)** Thin section of CD-11 sample, a fine-medium metasandstone with indicated directions of primary bedding (S_0) and orthogonal slaty cleavage (S_n). **D-E)** Thin section of CD-30A and CD-11 samples respectively showing very well preserved sedimentary grains and texture. **F)** XZ plane of sample CD-05 evidencing type σ quartz porphyroclast acting as a shear sense indicator, with top unit being thrusted to northeast.

4.2 Finite Strain

The new strain results provided in this study, reported in Table 1B and in Figure 8, illustrate the overall pattern of strain distribution in the Chapada Diamantina fold-and-thrust belt. Complete raw data are shown in the Appendix.

In the northeast part of the study area, the basement core is bounded by the Rio dos Remédios Group. The CD-01B sample is a high grade metamorphic rock, composed basically by quartz, plagioclase and K-feldspar from the Archean Gavião Complex. Two samples, CD-06A and CD-03A, come from the Rio dos Remédios Group, close to the contact with the crystalline basement by reverse shear zones. The CD-03A sample is an extremely foliated metarenite, with deformation of detrictic quartz grains subordinated to the main foliation (Novo Horizonte Formation). The CD-06A sample is a poorly sorted impure metarenite, from the Ouricuri do Ouro Formation, with sub-angular to sub-round quartz grains, oriented preferably, parallel to the preferred slaty cleavage. All these three samples show the highest values computed in this presented work.

Northwestwards of this region, in the western limb of the Piatã Brachysincline, sample CD-11, from the Açuruá Formation, is very close to the contact with Tombador Formation. The sample is a well sorted metarenite, with sub-angular to sub-rounded quartz grains, in which slaty cleavage is well marked and arranged perpendicularly to the bedding.

The CD-16 sample is a very fine metasiltite, with a very well-defined slaty cleavage, from the Ouricuri do Ouro Formation lying close to the hinge region of the Catolés anticline. For this sample, mud pellets were used as strain markers and, therefore, the rock's competence must be taken into account when evaluating the calculated deformation intensity.

Towards southwest, the CD-23 sample is a fine, well sorted metarenite, with sub-angular to sub-rounded single quartz grains, from the Açuruá Formation. It lies close to the hinge region of the Rio de Contas syncline. For this sample, more than 900 grains were processed and all sections yielded low shape ratios, ranging from 1.1 to 1.2.

In the western part of the study area, samples CD-30A and CD-28 are close to each other, lying near to a thrust fault, separating the Itaguaçu Anticline to east and the Érico Cardoso inverted Brachysincline to west. The CD-30A sample is a fine, well sorted quartz-metarenite from the Ouricuri do Ouro Formation and the CD-28 sample is a fine, well sorted, mature quartz-metarenite from the Açuruá Formation. Both show an overall low strain magnitude.

At the most southwestern region of the study area, sample CD-40 from the Serra da Gameleira formation (pre-rift phase sedimentation) lies near a major thrust fault system, which thrusts the basement units on top of the sedimentary cover towards northeast. The sample is from a well-sorted metarenite, with lepid-granoblastic texture, with low strain ratio values.

While in the most of the thin sections single quartz grains were used as strain markers, the samples CD-01B and CD-16 used ilmenite crystals and mud-pellets, respectively. The total intensity from sample CD-01B agrees with the distribution of the computed data, but the intensity parameter computed by CD-16 lies very far from other data.

Table 1: Three Dimensional (3D) Strain Data - Best Fit Ellipsoid

Panel A: Positional and lithologial data for each sample and axial length for the best-fit ellipsoid reported as Stretch (S).

Sample Code	Location		Map Unit	Lithology	Axial length		
	Longitude	Latitude			X $\pm 2\sigma$	Y $\pm 2\sigma$	Z $\pm 2\sigma$
CD-01B	41º 40' 09.2" S	13º 16' 11.7" W	Gavião Complex	Orthogneisse	1.314 $\pm$ 0.188	1.025 $\pm$ 0.125	0.746 $\pm$ 0.023
CD-03A	41º 35' 33.3" S	13º 16' 11.7" W	Novo Horizonte Fm.	Meta-sandstone	1.232 $\pm$ 0.059	1.055 $\pm$ 0.029	0.770 $\pm$ 0.017
CD-06A	41º 43' 05.1" S	13º 16' 36.0" W	Ouricuri do Ouro Fm.	Meta-sandstone	1.185 $\pm$ 0.044	1.085 $\pm$ 0.035	0.778 $\pm$ 0.024
CD-11	41º 56' 12.5" S	13º 05' 21.6" W	Açuruá Fm.	Meta-sandstone	1.141 $\pm$ 0.043	1.047 $\pm$ 0.034	0.838 $\pm$ 0.019
CD-16	42º 02' 13.4" S	13º 06' 54.6" W	Ouricuri do Ouro Fm.	Meta-siltstone	1.466 $\pm$ 0.082	1.165 $\pm$ 0.055	0.586 $\pm$ 0.013
CD-23	42º 00' 58.9" S	13º 18' 41.4" W	Açuruá Fm.	Meta-sandstone	1.219 $\pm$ 0.045	0.962 $\pm$ 0.034	0.854 $\pm$ 0.023
CD-28	42º 03' 37.5" S	13º 25' 30.8" W	Açuruá Fm.	Meta-sandstone	1.084 $\pm$ 0.009	1.013 $\pm$ 0.021	0.911 $\pm$ 0.017
CD-30A	42º 03' 28.3" S	13º 25' 15.6" W	Ouricuri do Ouro Fm.	Meta-sandstone	1.087 $\pm$ 0.026	1.049 $\pm$ 0.029	0.877 $\pm$ 0.014
CD-40	42º 12' 55.5" S	13º 26' 13.7" W	Serra da Gameleira Fm.	Meta-sandstone	1.116 $\pm$ 0.037	1.001 $\pm$ 0.032	0.896 $\pm$ 0.029

Panel B: Ellipsoid main parameters

Sample Code	$\sqrt{\bar{F}}$*	ϵ_s**	2σ (ϵ_s)	ν***	Flinn's K	2σ (K)	X/Z ratio	2σ (X/Z)	Ellipsoid Shape
CD-01B	5.3%	0.383	0.010	0.363	0.896	1.248	1.765	0.296	Oblate
CD-03A	7.6%	0.374	0.040	0.452	0.455	0.254	1.602	0.112	Oblate
CD-06A	3.6%	0.305	0.040	0.841	0.238	0.778	1.525	0.094	Oblate
CD-11	3.0%	0.222	0.010	0.328	0.375	0.350	1.362	0.071	Oblate
CD-16	2.2%	0.637	0.010	0.463	0.265	0.147	2.504	0.117	Oblate
CD-23	2.2%	0.227	0.006	-0.316	2.288	1.749	1.428	0.077	Prolate
CD-28	1.6%	0.116	0.001	0.441	0.668	0.566	1.190	0.024	Oblate
CD-30A	2.5%	0.158	0.010	0.712	0.203	0.335	1.241	0.037	Oblate
CD-40	3.3%	0.133	0.001	0.207	1.078	0.846	1.245	0.072	Oblate

*$\sqrt{\bar{F}}$ is the Incompatibility Index;
**ϵ_s is octahedral shear strain;
***ν is the Lode's ratio, which quantifies the strain ellipsoid's shape.

Panel C: Axial Orientation for best fit ellipsoids.

Sample Code	X Orientation		Y Orientation		Z Orientation	
	Trend $\pm$ 2σ (º)	Plunge $\pm$ 2σ (º)	Trend $\pm$ 2σ (º)	Plunge $\pm$ 2σ (º)	Trend $\pm$ 2σ (º)	Plunge $\pm$ 2σ (º)
CD-01B	149.8 $\pm$ 13.6	66.5 $\pm$ 8.0	357.5 $\pm$ 17.0	20.6 $\pm$ 12.6	026.8 $\pm$ 17.6	09.8 $\pm$ 5.5
CD-03A	099.4 $\pm$ 06.4	42.7 $\pm$ 1.6	329.2 $\pm$ 06.4	34.9 $\pm$ 04.4	218.0 $\pm$ 04.6	27.4 $\pm$ 2.0
CD-06A	260.9 $\pm$ 68.3	45.7 $\pm$ 4.9	351.8 $\pm$ 68.2	00.7 $\pm$ 04.0	082.4 $\pm$ 05.9	44.3 $\pm$ 2.2
CD-11	274.8 $\pm$ 34.5	33.1 $\pm$ 5.0	176.8 $\pm$ 34.5	12.4 $\pm$ 09.9	068.7 $\pm$ 10.6	54.1 $\pm$ 3.5
CD-16	307.0 $\pm$ 16.2	64.4 $\pm$ 3.2	163.2 $\pm$ 16.1	21.1 $\pm$ 01.3	067.8 $\pm$ 03.4	13.7 $\pm$ 1.1
CD-23	177.2 $\pm$ 05.5	36.0 $\pm$ 3.1	032.7 $\pm$ 06.4	48.2 $\pm$ 05.0	281.1 $\pm$ 06.3	18.3 $\pm$ 3.6
CD-28	111.2 $\pm$ 18.0	70.8 $\pm$ 3.4	335.4 $\pm$ 17.9	14.1 $\pm$ 07.3	241.9 $\pm$ 07.6	12.9 $\pm$ 4.0
CD-30A	293.5 $\pm$ 54.1	33.2 $\pm$ 7.1	154.5 $\pm$ 54.1	49.1 $\pm$ 07.0	038.7 $\pm$ 07.9	21.3 $\pm$ 6.5
CD-40	155.7 $\pm$ 22.6	38.7 $\pm$ 7.5	020.9 $\pm$ 23.7	41.1 $\pm$ 20.3	267.9 $\pm$ 22.3	24.8 $\pm$ 9.2

The intensity of deformation for the 3D ellipsoids represented by the strain ratio (X/Z) varies from 1.19 to 2.504 with average uncertainty of 0.1 (octahedral shear strain ϵ_s, varying from 0.116 to 0.383) (Table 1B). The sample CD-16 shows the highest strain ratio X/Z equals to 2.504, far from other intensity data computed (Table 1 and Fig. 9A-B). Sample CD-16 is the only meta-siltstone analysed, where the strain markers were not single quartz grain, but mud pellets.

The very high strain intensity computed by CD-16 sample may provide a general idea of the strain intensity values in the most incompetent layers, while the competent units have a strain intensity very well constrained by all other computed samples.

Most of the best-fit ellipsoids have an oblate shape (k<1, ν Lode's ratio > 0), with the exception of sample CD-23 with a prolate shape ($k > 1$, ν Lode's ratio < 0). However, samples CD-40 and CD-01B can be approximated to a plane strain shape ($k \approx 1$, ν Lode's ratio ≈ 0)((Fig. 9A-B).

Regarding axial orientations, the Z and Y strain ellipsoid axes are well constrained with small variability in orientation, while the X axis shows a little more dispersed pattern (Fig. 9C). Z axes exhibit a mean ENE sub-horizontal orientation compatible with a steep NNW flattening mean plane, and Y axes show a NNW sub-horizontal orientation. Although the X axes are more dispersed, its mean orientation is near down-dip regarding the mean flattening plane, and the dispersion is due to the CD-06A, CD-11, CD-30A and CD-16 samples which are the most oblate and thus have a well defined flattening plane with less defined X and Y axes (Table 1C).

Since the cross-section is generally drawn parallel to Z axes of the samples, the Z axial length, reported as stretch in Table 1A, will be used to calculate the amount of shortening by the strain integration technique (Hossack, 1978; Woodward et al., 1986). After computing the original length by Eq. 1, the amount of shortening was calculated by the elongation equation (Eq. 2), yielding a total of 21.65% of shortening.

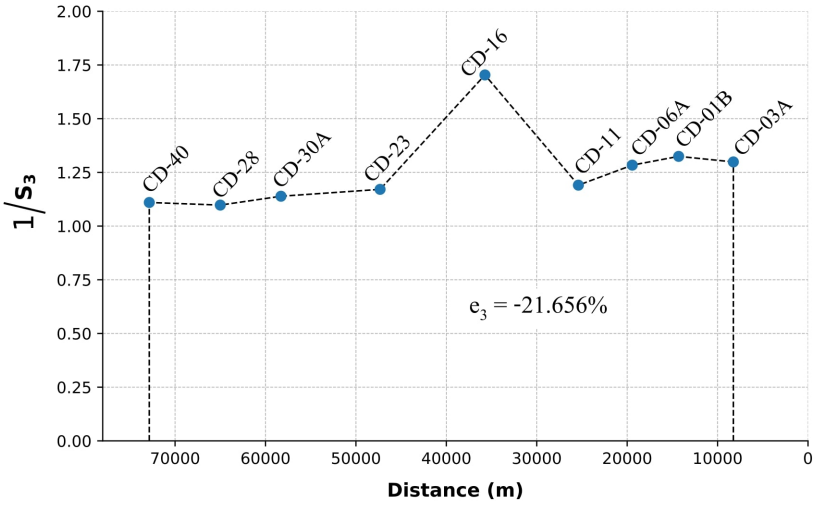

Figure 7: Finite strain trajectory integration: plot of the reciprocal stretch of Z axes along the section trajectory, where the area under the curve is the original length of the strain trajectory.

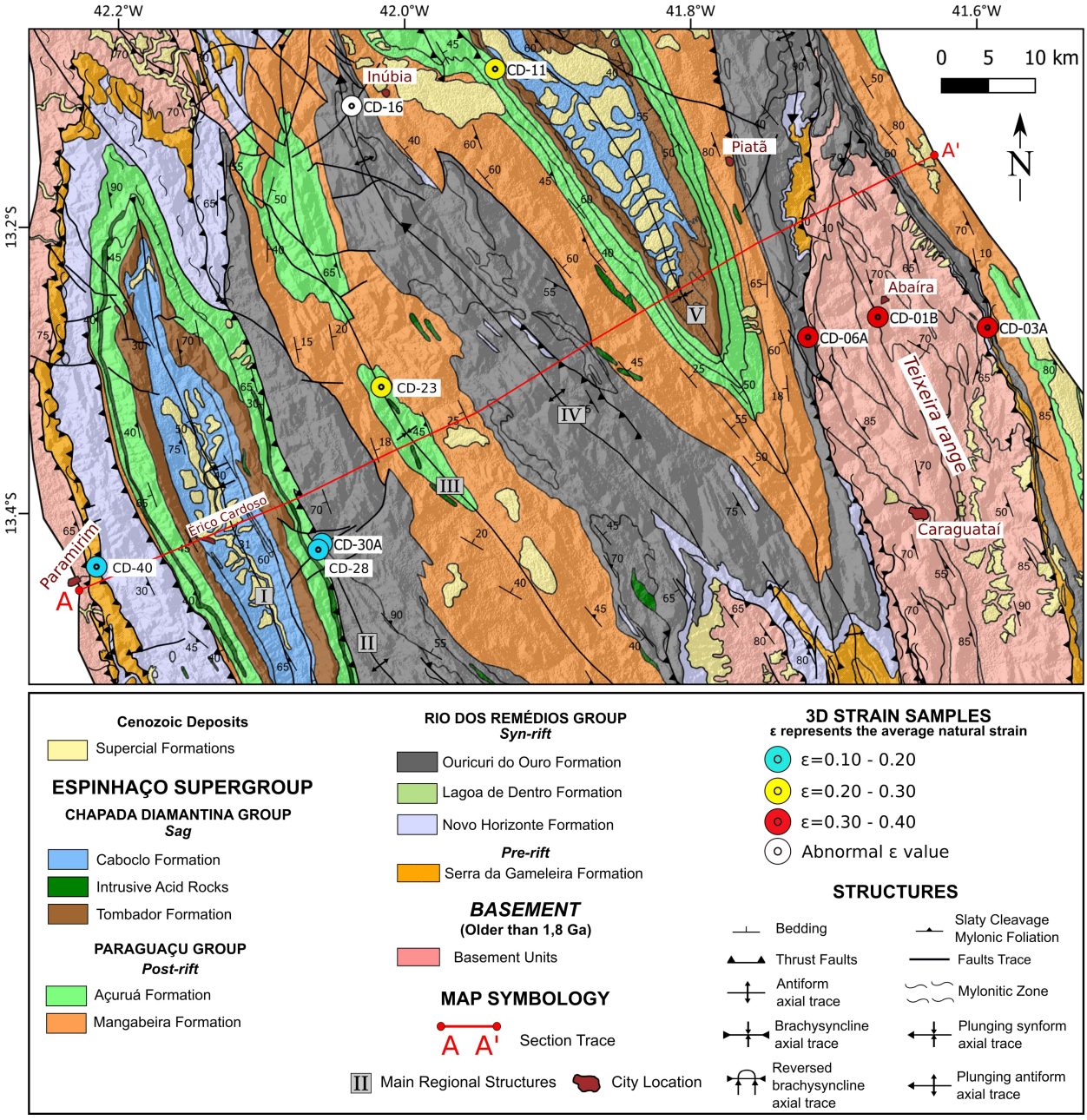

Figure 8: Geological map of the studied area overlaid on digital elevation model with location of strain samples presented in this study (modified from Guimarães et al. (2008). I: Érico Cardoso Brachysyncline; II: Itaguaçu Anticline; III: Rio de Contas Syncline; IV: Catolés Anticline; V: Piatã Brachysyncline.

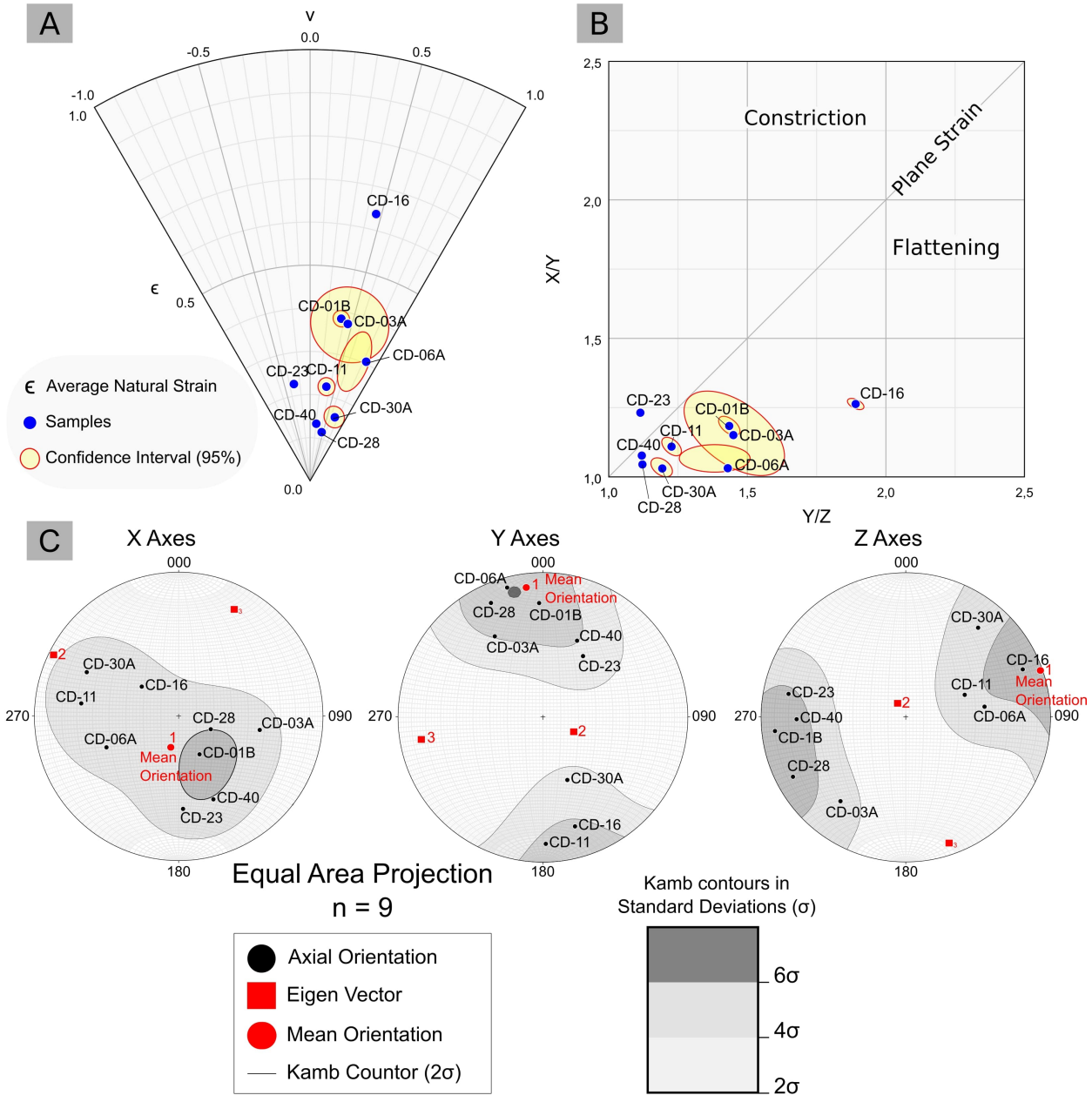

Figure 9: A: The Nadai-Hsü Plot; **B:** Flinn Diagram representing the ellipsoid's shape with 95% confidence interval. **C:** 3D finite strain ellipsoid X-, Y- and Z-axial orientations. Black points are axial orientations for all samples, Kamb contours are filled in gray scale at 2σ intervals and red numbered square are Bingham axial distribution eigenvectors. (Low-hemisphere equal-area stereograms and Bingham parameters produced using Stereonet 11 (Allmendinger et al., 2011; Cardozo and Allmendinger, 2013), Flinn and Nadai-Hsü plots by *EllipseFit* (Vollmer, 2018);

4.3 Geological Model

In this section, we present and describe the structural styles proposed for the study area, based on the forward models (Fig. 10) and structural balancing process of the main section (Fig. 11). The proposed section runs across the Chapada Diamantina Fold and Thrust Belt (FTB) involving large thin- and thick-skinned structures.

Based on the forward models, the origin of the Chapada Diamantina FTB can be geometrically and kinematic explained by the reactivation of minor and major extensional normal faults separating structural highs and grabens in an initial rift type sedimentary basin. Although not shown here, the model was built since extensional phases, where we applied simple shear algorithm to simulate extension with syn-subsidence sedimentation. After rifting phase, a short phase of erosion is applied on top of the syn-rift to construct the unconformity between syn- and post-rift sedimentation (Fig. 10a).

The tectonic inversion process begins with the reactivation of the two easternmost faults, where fault (1) is responsible for uplifting the major Archean block comprising the Teixeira range (Fig 10b). The following stage depicts back-thrusts with basement uplift and associated folding of sedimentary cover by possible reactivation of minor buried normal faults (3) and reactivation of extensional faults (4 and 5) as reverse (Fig. 10c).

In order to model the Érico Cardoso overturned syncline, new thrust faults were modelled to account for thick-skinned tectonics represented by fault (6), a footwall shortcut thrust (Fig. 10d). The propagation of fault 7 is responsible for more folding onto the structure and overturning the syncline. Using a topographic line similar to the present configuration, the model display similar overall structural distribution of the study area (Fig. 10e).

Having the subsurface structural scenario presented by the forward models and respecting available surface data of the geological maps, balanced cross sections were constructed oriented orthogonally to the main structures (Fig. 11a). The proposed cross section is approximately 77 kilometers long with an average vertical thickness of 5,564 meters for the sedimentary package.

Our cross section (Fig. 11a) infers a major décollement level at 21 km deep within the crystalline basement where reactivated normal faults detach. Additionally, the model supposes the reactivation of normal faults as reverse, but also depicts shallow thrusts within the sedimentary cover, without involving the basement, specially in the Catolés Anticline (Fig 11a).

Thickness variation occurs mainly with the syn-rift units, Novo Horizonte and Ouricuri do Ouro formations, with thickening close to the hanging walls of normal faults. The restored cross section shows a horst and graben basins architecture reflected by the basement, with a increased depositional space in the center of the model.

The comparison between the present day interpretation and restored cross section show a difference of 18.6 kilometers. This value yields a total of 19.37% of shortening, understood as the minimum tectonic shortening for the proposed model (Fig. 11b).

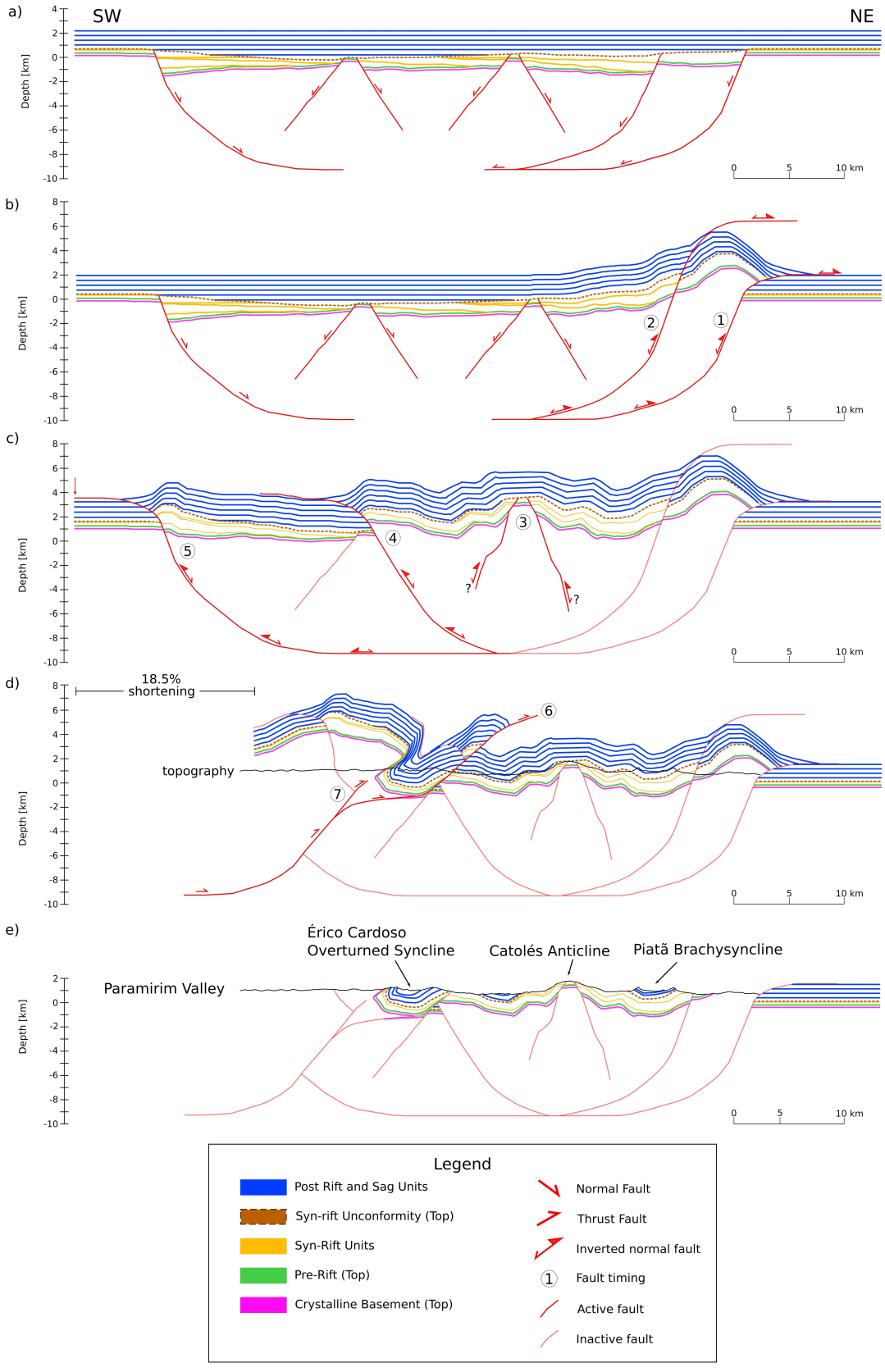

Figure 10: Forward modelling of section. Geological evolution is described in text. We warn the reader that the proposed model stops just after the outcropping basement core in the Teixeira range, and consequently the presented easternmost horizontal beds do not represent the actual geology of the area, but it is rather an artifact of the model. See Guimarães et al. (2008) for more details of the regional main geological structures.

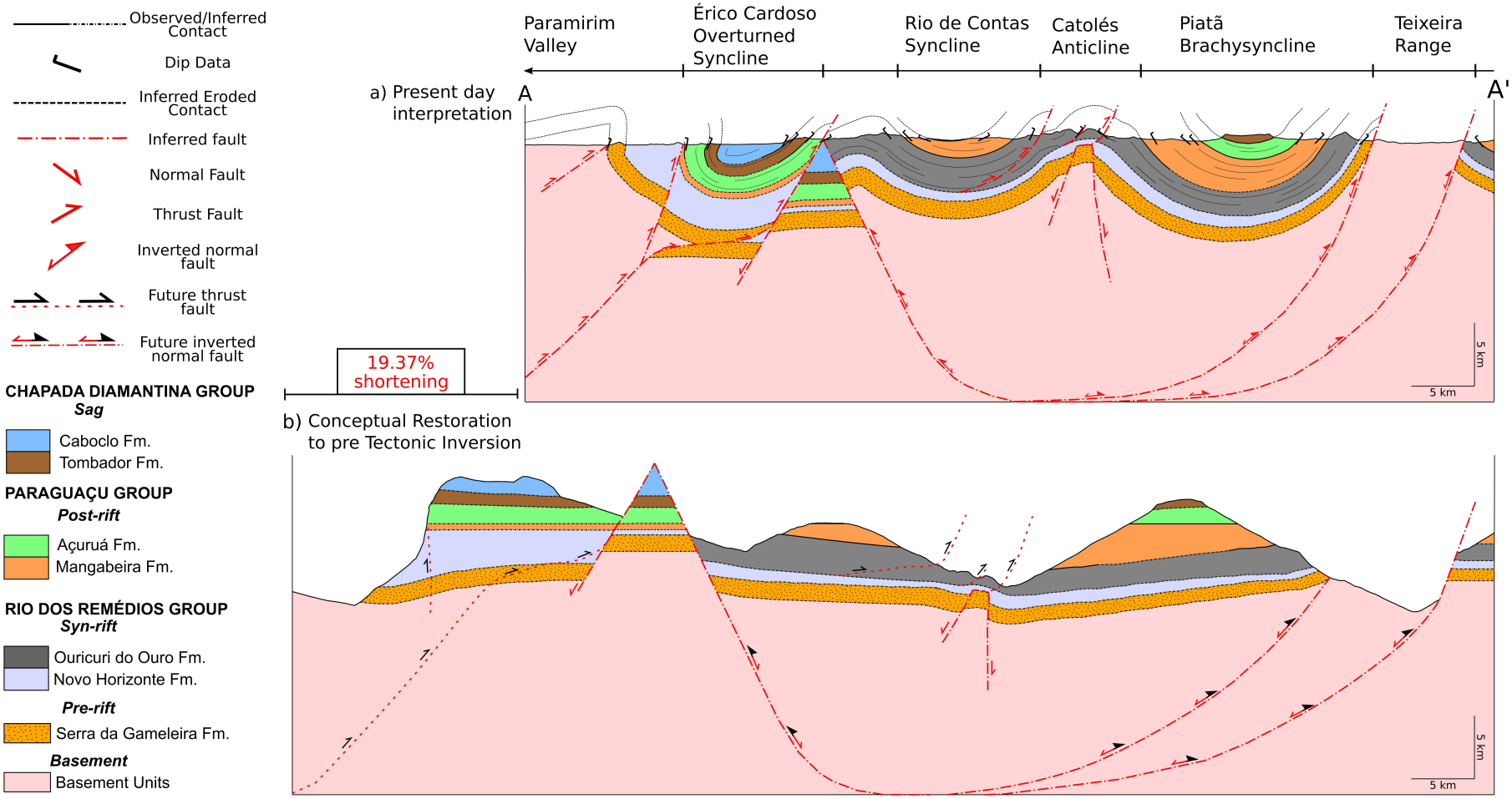

Figure 11: Balanced and restored cross-sections through the Chapada Diamantina Fold and thrust belt. **(a)** Present day interpretation of geological cross section. See Fig. 8; **(b)** Conceptual restored cross section to pre tectonic inversion of the Paramirim aulacogen. The comparison with the balanced section yields a minimum tectonic shortening of 19.37%.

5 DISCUSSION

5.1 Finite Strain

In order to use the Inertia Tensor method for finite strain analysis, here utilized by the shape preferred orientation (SPO) software (Launeau and Cruden, 1998), at least two assumptions should be fulfilled. The initial shape of the deformed objects should be approximately equidimensional (tending to be circular or spherical), and the deformation has be passive, i.e. there was no viscosity contrast between the measured objects and their interstitial matrix.

We consider that these conditions have been met in the present work, since (i) mainly quartz grains in metasandstones were analysed, which original sedimentary grains shape may be assumed as approximately spherical; (ii) rock matrix has a similar mineralogical composition, leading to a non rheological contrast with quartz grains. Even the samples CD-01B and CD-16, in which ilmenite crystals and mud-pellet were respectively used, these conditions were fulfilled.

Furthermore a good agreement was obtained between the ellipsoid axis and the field measured for flattening foliations and stretching lineations (compare figures 5 and 9C) leading to a steep NNW striking and SW dipping flattening plane with nearly down-dipping main stretching direction. It should be noted that the applied strain techniques were completely independent from the field foliation and lineation measures.

The higher strain ratios were obtained in samples from northwest of the studied region, corresponding to a basement sample (CD-01B) or samples near to shear zones limiting the basement and the supracrustals rocks (CD-03A and CD-06A), while low to intermediate strain magnitudes are scattered along the sedimentary cover.

Anyway these results most probably represents a minimum strain values since mainly more rheological competent metasandstones sample were analysed while metapelitic and volcanic were subsampled, due the limitations of the applied techniques.

The oblate shape of most samples associated with down-dipping stretching directions could be interpreted as a transpressional regime (Sanderson and Marchini, 1984; Fossen et al., 1994; Fossen and Tikoff, 1998). Nevertheless, the possibility that the oblate shape is related to a volume loss cannot be totally ruled out, once pressure solution along the tectonic cleavages commonly occurs in low-grade metasedimentary rocks (Ramsay and Wood, 1973). More data and different approaches are needed to better constrain this specific question.

5.2 Geological Cross Section

The adopted model for the construction, balancing and restoration of the cross section assumes the reactivation of normal rift faults as reverse (steep thrust) faults, where the structural architecture of the area is mainly controlled by rift geometrical settings. In practice, this means that the initial normal faults served as anisotropies planes and started to act as reverse faults controlling the localization of thrust or serving as shortcut thrust ramps during the tectonic inversion

phase. Our model is consistent with this assumption as it reassembles the initial rift geometry when unfolding the section.

In the Chapada Diamantina region, the lack of seismic profiles and borehole data in addition to the complex initial stratigraphic geometry, comprising structural highs and grabens, impose a important limitation and high uncertainty in the recognition of deep structures. For this region, forward models were constructed to assess this assumptions and the results (Fig. 10) show geometrical and kinematical viability of the proposed model, reinforcing this assumption.

When balancing by the line length technique, after restoration the line lengths should not deviate more than 5% from the initial interpretation in order to fulfill the balance criteria to consider the section balanced, which is the case for our model (Lingrey and Vidal-Royo, 2015). Once all the other criteria, such as accuracy, admissibility and restorability, are achieved in our model it can considered balanced.

The rift architecture imposes several difficulties to also preserve thickness after restoration (area balancing the cross-section). This fact is mainly because some units are not horizontally continuous along the basin and vary in thickness, such as the Rio do Remédios Group (Fig. 11). Even so, the proposed model resulted in an average 5,564 meters thick stratigraphic package of the Espinhaço Supergroup. When compared to published data for the region and gravimetric basement topography models (D'Angelo et al., 2019) or to geological mapping survey report (Guimarães et al., 2008) the average thickness of the units may be considered as a reasonably compatible result.

Our model shows an expressive pile of volcanic rocks from the Novo Horizonte Formation under the Érico Cardoso Overturned syncline, which is constrained solely by geometric relationships from maps. We interpret this feature as the onset of the rifting phase with extended acid volcanic activity from partial melting of crustal older rocks (Guimarães et al., 2008; Teixeira, 2005). Eastward of this region, the restored section shows a meaningful accommodation space in which the Ouricuri do Ouro formation was deposited. This reflects the strong tectonic control in the interior of the basin, characterized by continental siliciclastic phases deposition restricted to grabens, with conglomerates rocks generated by gravitational flux close to normal faults, predominant fluvio-lacustrine depositional processes with high faciological variation and immature clastic deposits of the Ouricuri do Ouro Formation (Guimarães et al., 2008).

The contact with the upper marine/coastal unit, Mangabeira Formation, is a clear erosional and/or tectonic unconformity (Fig. 11b), marking the shift of tectonic regime of the basin. The restored post rift phase is in agreement with a sedimentation with no major tectonic activity and little lithofaciological variation within the sequence as reported by Guimarães et al. (2008). Finally, the basin is covered by continental deposits (eolian, fluvial and marine sediments) related to the Tombador and Caboclo formation, reflecting a sag sedimentation phase (Guimarães et al., 2008).

Our model incorporates an inferred basal detachment fault, around 21 km deep, separating the volcanic - sedimentary cover from the basement with the reactivation of inital rift faults as reverse controlling the cover folding. This allows the coexistence of thin- and thick-skinned deformation style, clearly shown in the Érico Cardoso overturned syncline and in the Teixeira range, respec-

tive. This interpretation is popular in the regional geological literature (Cruz and Alkmim, 2006). However additional studies are badly needed to investigate the possible existence of shallow detachment levels within the sedimentary cover.

The basement architecture and deep structures proposed in our model are favored by the work of D'Angelo et al. (2019), which show a general graben and horst geometry of the crystalline basement rock under the sedimentary cover, based on 3D Euler solutions from magnetic data. Therefore, the basement blocks were modelled with vertical to sub-vertical fault net slip controlled mainly by the ancient SW-NE normal faults. The rift interpreted paleo-relief of the Chapada Diamantina fold-and-thrust system shows regional "highs" and "lows" of the crystalline basement matching anticline, as the Serra do Barbado anticline, and synclines, as the Érico do Cardoso overturned syncline, respectively. This regional architecture is also consistent in the proposed forward models (Fig. 10e).

In our model, the overall geometry and kinematic evolution of the system is well constrained as possible, allowing us to obtain robust results in the structural-geometric reconstruction of the Western Chapada Diamantina fold-and-thrust system. However, we acknowledge that the style of thick-skinned structures in subsurface represents a large source of uncertainty, since the contact between the crystalline basement and the sedimentary cover has not been fully mapped to verify the geometric relationships. Another source of uncertainty may be the assumption of plane strain, inherent to the concept of section balancing, when there are clear structural evidences of N-S contractional event affecting the fold-and-thrust system (Cruz and Alkmim, 2006, 2017).

5.3 Estimated shortening across the section

Three different and independent approaches were applied to estimate the tectonic shortening in the section: integration of ductile finite strain across the section (Fig. 7), restoration of the balanced section (Fig. 11) and the assessment of forward models (Fig. 10).

The calculation of 21.65% of shortening provided by the integration of the finite strain represents the horizontal component of ductile flattening strain across the section. It's an estimation of regional strain and the component of shortening due to penetrative strain, representing a minimum shortening value as body rotation is not considered (Woodward et al., 1986; Hossack, 1978).

The balanced cross-section was restored by flexural slip folding mechanisms, which maintains bed thickness. This procedure include the displacement associated with faults, bed rotation by the flexural slip and the ductile strain flattening associated with the unfolding. Thus, the amount of 19.37% of shortening from cross-section restoration and unfolding represents the minimal magnitude of deformation. The 18.5% of tectonic shortening estimated by the forward model follows the same principles and can be used to estimate the amount of deformation.

These are the first attempts to estimate the amount of shortening affecting the area and they provide new insights to investigate the evolution of the Paramirim aulacogen and the São Francisco craton. However, our model does not take in account the transverse deformation in a major SE-

NW direction, orthogonal to the section plane, as proposed by (Cruz and Alkmim, 2006), assuming a major plane strain deformation, in order to apply the balancing techniques.

5.4 Regional Tectonic Implications

The field and petrographic evidence, as well as the cross-section modelling indicate the basement involvement in the deformation of the Western Chapada Diamantina, i.e. a thick-skinned tectonic style, with the basement been thrusted over the volcanic-sedimentary cover in different areas of the section.

The amount of shortening estimated for the Western Chapada Diamantina region rises questions about the role of the Paramirim corridor during the Brasiliano orogeny. The Paramirim corridor is composed by two marginal and opposed vergent fold-and-thrust belts, the northern Espinhaço range on the west, the Chapada Diamantina region on east, with a central metamorphic high-grade block uplifted in the Paramirim valley. Thus the total amount of shortening across the Paramirim aulacogen might be much greater than the estimated range of tectonic shortening between 18-22% at the Western Chapada Diamantina region. As a consequence, we can assume that the western and eastern parts of the São Francisco craton could not be considered as rigidly linked during the Neoproterozoic - Cambrian Brasiliano orogeny.

Structural inheritance can be considered one of the main boundary conditions conducting the development of basement involved fold and thrust belts within cratonic domains (Butler et al., 2006). In the Paramirim corridor, structural inheritance from Paleoproterozoic terrane amalgamation is definitive, where older crystalline basement structures and geometry controlled basin formation and the inversion tectonics (Martins-Ferreira, 2019; D'Angelo et al., 2019). Interesting point is that structural trends in the older 1.8 Ga basement (Gavião and Paramirim complexes) and in the volcanic-sedimentary cover (Espinhaço Supergroup) are strictly parallel (see Fig. 5), although developed in very different metamorphic grades.

According to Butler et al. (2006), cratons are assumed to have lower heat flow and thicker lithospheric mantle, and therefore would have a higher resistance, comparing to young rifted continental lithosphere, with a thin mantle component. Nonetheless, this is not true for the SFC in the studied region, where shortening efficiently propagated into continental crust reaching domains regarded as intracratonic (Martins-Ferreira, 2019). Lacombe and Bellahsen (2016) proposed that tectonic inversion occurring in far-foreland domains commonly relies upon specific boundary conditions to ensure efficient transmission of stress and propagation of deformation, such as thermal, structural and/or compositional inheritance or weakening as key factors.

As the rheology of continental lithosphere appears to be an important factor in deformational processes, models show that rock viscosity are extremely sensitive to temperature (Hansen and Nielsen, 2003). Thus, regional increase of temperature might be the cause for physical weakening of the craton, and consequently fault reactivation in crystalline basement and folding, as the cratonic domains becomes efficient in lithospheric stress transmission (Martins-Ferreira, 2019). The

rising of temperature across the Paramirim aulacogen is evidenced by the Late Ediacaran and Cambrian K-Ar and Ar-Ar ages (Cordani, 1973*a*; Süssenberger et al., 2014).

Ultimately, we want to reinforce that the estimated range of minimum tectonic shortening between 18-22% at the Western Chapada Diamantina region is an important result that can provide new parameters to future research of the kinematical and geological evolution of the São Francisco craton and related orogens.

5.5 Future Developments

Some issues need future approaches to better constrain the discussion involved:

i. The relationships and contacts between the basement and cover deserve be better studied. Particularly the metamorphic contrast between both having the same structural trend is an intriguing question;

ii. Stratigraphic variation and maximum thickness must be further investigate to provide new kinds of constraints to the model;

iii. The deformation regime, i.e. the relative proportions of pure and simple shear could be achieved by vorticity analysis techniques, using for example quartz C-axis patterns;

iv. New models supposing shallower detachment levels within the sedimentary sequence would also be constructed and tested and compared with the here presented model;

v. Since our model does not take in account the transverse deformation regarding the studied cross-section, assuming a major plane strain deformation, new sections can be constructed in order to make a three-dimensional model;

vi. Construct more sections across the entire Paramirim aulacogen.

6 CONCLUSIONS

This work, carried out in the Western Chapada Diamantina fold-and-thrust belt, presents the results of strain analyses, the entire process of construction, balancing and restoration of a geological cross-section and the use of forward models as well. The results show a direct geometric relationship between the inversion of normal faults related to rifting settings and the development of thrusts faults, responsible for the deformation and folding of the sedimentary cover. The key findings from this study can be summarized below:

(i) The intensity of deformation for the 3D ellipsoids represented by the strain ratio (X/Z) vary from 1.190 to 2.504 with average uncertainty of 0.1 (octahedral shear strain ϵ_s, varying from 0.116 to 0.637). Most of the best-fit ellipsoids have an oblate shape (k<1, ν Lode's ratio > 0), with the exception of one sample with a prolate shape ($k > 1$, ν Lode's ratio < 0) and two that are more close to a plane strain ($k \approx 1$, ν Lode's ratio ≈ 0);

(ii) A good agreement was obtained between the ellipsoid axis and the field measured for flattening foliations and stretching lineations leading to a steep NNW striking and SW dipping flattening plane with nearly down-dipping main stretching direction;

(iii) The higher strain ratios were obtained in samples from eastward of the studied region, corresponding to a basement sample or samples near to shear zones limiting the basement and the supracrustals rocks, while low to intermediate strain magnitudes are scattered along the sedimentary cover. These results represents a minimum strain values since mainly more rheological competent metasandstones sample were analysed while metapelitic and volcanic were subsampled, due the limitations of the applied techniques;

(iv) Three different and independent approaches (finite strain analyses, cross section restoration and forward modelling) were applied to estimate the tectonic shortening in the section resulting in a range of tectonic shortening between 18-22% at the Western Chapada Diamantina region. These results represents a minimum shortening values;

(v) The amount of shortening estimated for the Western Chapada Diamantina region rises questions about the role of the Paramirim corridor during the Brasiliano orogeny. As the Western Chapada Diamantina corresponds to the eastern branch of the Paramirim corridor, which is also composed by the Northern Espinhaço range toward west and the central uplifted basement of the Paramirim valley, the total amount of shortening across the Paramirim inverted aulacogen might have been greater than the estimated range of 18-22% at the Western Chapada Diamantina. Thus the western and eastern parts of the São Francisco craton could not be considered as rigidly linked during the Neoproterozoic - Cambrian Brasiliano orogeny, in which the Paramirim aulacogen exerted an import role into the mobility of the São Francisco craton.

7 BIBLIOGRAPHY

Alkmim, F. F., Marshak, S., Fonseca, M. A., 2001, Assembling West Gondwana in the Neoproterozoic: clues from the Sao Francisco craton region, Brazil: Geology, v. 29, no. 4, p. 319–322, doi:10.1130/0091-7613(2001)029<0319:AWGITN>2.0.CO;2.

Alkmim, F. F., Marshak, S., Pedrosa-Soares, A. C., Peres, G. G., Cruz, S. C. P., Whittington, A., 2006, Kinematic evolution of the Araçuaí-West Congo orogen in Brazil and Africa: Nutcracker tectonics during the Neoproterozoic assembly of Gondwana: Precambrian Research, v. 149, no. 1-2, p. 43–64, doi:10.1016/j.precamres.2006.06.007.

Alkmim, F. F., Martins-Neto, M. A., 2012, Proterozoic first-order sedimentary sequences of the São Francisco craton, eastern Brazil: Marine and Petroleum Geology, v. 33, no. 1, p. 127–139, doi:10.1016/j.marpetgeo.2011.08.011.

Allmendinger, R. W., Cardozo, N., Fisher, D. M., 2011, Structural geology algorithms: Vectors and Tensors in Structural Geology: New York, Cambridge University Press, 304 p.

Almeida, F. F. M., 1977, O cráton do São Francisco: Revista Brasileira de Geociências, v. 7, no. 4, p. 349–364.

Almeida, F. F. M., de Brito Neves, B. B. d., Carneiro, C. D. R., 2000, The origin and evolution of the South American Platform: Earth-Science Reviews, v. 50, no. 1-2, p. 77–111, doi:10.1016/S0012-8252(99)00072-0.

Barbosa, J. S. F., Sabaté, P., 2004, Archean and Paleoproterozoic crust of the São Francisco craton, Bahia, Brazil: geodynamic features: Precambrian Research, v. 133, no. 1-2, p. 1–27, doi:10.1016/j.precamres.2004.03.001.

Barbosa, J. S., Sabaté, P., 2002, Geological features and the Paleoproterozoic collision of four Archean crustal segments of the São Francisco Craton, Bahia, Brazil: a synthesis: Anais da Academia Brasileira de Ciências, v. 74, no. 2, p. 343–359, doi:10.1590/S0001-37652002000200009.

Brito Neves, B. B. d., Campos Neto, M. D. C., Fuck, R. A., 1999, From Rodinia to Western Gondwana: an approach to the Brasiliano-Pan African Cycle and orogenic collage: Episodes, v. 22, no. 3, p. 155–199.

Butler, R. W., Tavarnelli, E., Grasso, M., 2006, Structural inheritance in mountain belts: an Alpine–Apennine perspective: Journal of Structural Geology, v. 28, no. 11, p. 1893–1908, doi:10.1016/j.jsg.2006.09.006.

Campos Neto, M. C., 2000, Orogenic Systems from Southwestern Gondwana: an approach to Brasiliano–Pan African Cycle and orogenic collage in Southeastern Brazil, *in* Cordani, U. G., Milani, E. J., Thomaz Filho, A., Campos, D. A., org., Tectonic Evolution in South America, Rio de Janeiro: s.n., p. 335–365.

Cardozo, N., Allmendinger, R. W., 2013, Spherical projections with OSXStereonet: Computers & Geosciences, v. 51, p. 193–205, doi:10.1016/j.cageo.2012.07.021.

Cavalcante, C., Fossen, H., Almeida, R. P., Hollanda, M. H. B., Egydio-Silva, M., 2019, Reviewing the puzzling intracontinental termination of the Araçuaí-West Congo orogenic belt and its implications for orogenic development: Precambrian Research, v. 322, p. 85–98, doi:10.1016/j.precamres.2018.12.025.

Cordani, U. G., 1973*a*, Definição e caracterização do Cráton do São Francisco, in Congresso Brasileiro de Geologia. Aracaju, Vol. 2, p. 142–145.

Cordani, U. G., 1973*b*, Evolução geológica pré-cambriana da faixa costeira do Brasil entre Salvador e Vitória. [Tese Livre Docência]: Universidade de São Paulo, 98 p.

Cordani, U. G., 1978, Comentários Filosóficos Sobre Evolução Geológica Pré-Cambriana: Salvador, SBG/NBA, v. 3, p. 33–65.

Cordani, U. G., Iyer, S. S., Taylor, P. N., Kawashita, K., Sato, K., McReath, I., 1992, Pb-Pb, Rb-Sr, and K-Ar systematics of the Lagoa Real uranium province (south-central Bahia, Brazil) and the Espinhaço cycle (ca. 1.5-1.0 Ga): Journal of South American Earth Sciences, v. 5, no. 1, p. 33–46, doi:10.1016/0895-9811(92)90058-7.

Costa, L. A. M., Inda, H. A. V., 1982, O aulacógeno do Espinhaço: Ciências da Terra, v. 2, p. 13–18.

Cruz, S. C., Alkmim, F. F., 2006, The tectonic interaction between the Paramirim aulacogen and the Araçuaí belt, São Francisco craton region, Eastern Brazil: Anais da Academia Brasileira de Ciencias, v. 78, no. 1, p. 151–173, doi:10.1590/s0001-37652006000100014.

Cruz, S. C. P., Alkmim, F. F., 2017, The Paramirim Aulacogen, *in* Heilbron, M., Cordani, U. G., Alkmim, F. F., org., São Francisco Craton, Eastern Brazil: Tectonic Genealogy of a Miniature Continent, Springer, p. 97–115.

Cruz, S. C. P., Alkmim, F. F., Barbosa, J. S. F., Dussin, I., Gomes, L. C. C., 2015, Tectonic inversion of compressional structures in the Southern portion of the Paramirim Corridor, Bahia, Brazil: Brazilian Journal of Geology, v. 45, no. 4, p. 541–567, doi:10.1590/2317-488920150030240.

Cruz, S. C. P., Barbosa, J. S. F., Pinto, M. S., Peucat, J.-J., Paquette, J. L., de Souza, J. S., de Souza Martins, V., Júnior, F. C., Carneiro, M. A., 2016, The Siderian-Orosirian magmatism in the Gavião Paleoplate, Brazil: U–Pb geochronology, geochemistry and tectonic implications: Journal of South American Earth Sciences, v. 69, p. 43–79, doi:/10.1016/j.jsames.2016.02.007.

Cruz, S. C. P., Dias, V. M., Alkmim, F. F., 2007, A interação tectônica embasamento/cobertura em aulacógenos invertidos: um exemplo da Chapada Diamantina Ocidental: Revista Brasileira de Geociências, v. 37, no. 4 suppl, p. 111–127.

Dahlstrom, C. D. A., 1969, Balanced cross sections: Canadian Journal of Earth Sciences, v. 6, no. 4, p. 743–757, doi:10.1139/e69-069.

Danderfer, A., Dardenne, M. A., 2002, Tectonoestratigrafia Da Bacia Espinhaço na porção centro-norte do Cráton Do São Francisco: registro de uma evolução poliistórica descontínua: Revista Brasileira de Geociências, v. 32, no. 4, p. 449–460, doi:10.25249/0375-7536.2002324449460.

Danderfer, A., De Waele, B., Pedreira, A. J., Nalini, H. A., 2009, New geochronological constraints on the geological evolution of Espinhaço basin within the São Francisco Craton—Brazil: Precambrian Research, v. 170, no. 1-2, p. 116–128, doi:10.1016/j.precamres.2009.01.002.

Danderfer Filho, A., 1990, Análise estrutural descritiva e cinemática do Supergrupo Espinhaço na região da Chapada Diamantina (BA) [Tese de Mestrado]: Universidade Federal de Ouro Preto.

D'Angelo, T., Barbosa, M. S. C., Danderfer Filho, A., 2019, Basement controls on cover deformation in eastern Chapada Diamantina, northern São Francisco Craton, Brazil: Insights from potential field data: Tectonophysics, v. 772, p. 228231, doi:10.1016/j.tecto.2019.228231.

Elliott, D., 1983, The construction of balanced cross-sections: Journal of Structural Geology, v. 5, no. 2, p. 101, doi:10.1016/0191-8141(83)90035-4.

Faleiros, F. M., 2008, Evolução de Terrenos Tectono-Metamórficos da Serrania do Ribeira e Planalto Alto Turvo (SP, PR) [Tese de Doutorado]: Universidade de São Paulo, 306 p.

Fossen, H., Cavalcante, C., Konopásek, J., Meira, V. T., Almeida, R. P., Hollanda, M. H. B., Trompette, R., 2020, A critical discussion of the subduction-collision model for the Neoproterozoic Araçuaí-West Congo orogen: Precambrian Research, v. 343, p. 105715, doi:10.1016/j.precamres.2020.105715.

Fossen, H., Tikoff, B., 1998, Extended models of transpression and transtension, and application to tectonic settings: Geological Society, London, Special Publications, v. 135, no. 1, p. 15–33, doi:10.1144/GSL.SP.1998.135.01.02.

Fossen, H., Tikoff, B., Teyssier, C., 1994, Strain modeling of transpressional and transtensional deformation: Norsk geologisk tidsskrift, v. 74, no. 3, p. 134–145.

Groshong Jr, R. H., 2006, 3-D Structural Geology: Heidelberg, Springer-Verlag, 400 p.

Guadagnin, F., Chemale Jr., F., 2015, Detrital zircon record of the Paleoproterozoic to Mesoproterozoic cratonic basins in the São Francisco Craton: Journal of South American Earth Sciences, v. 60, p. 104–116, doi:10.1016/j.jsames.2015.02.007.

Guadagnin, F., Chemale Jr, F., Magalhães, A. J. C., Santana, A., Dussin, I., Takehara, L., 2015, Age constraints on crystal-tuff from the Espinhaço Supergroup—Insight into the Paleoproterozoic to Mesoproterozoic intracratonic basin cycles of the Congo–São Francisco Craton: Gondwana Research, v. 27, no. 1, p. 363–376, doi:10.1016/j.gr.2013.10.009.

Guimarães, J. T., Alkmim, F. F., Cruz, S. C. P., 2012, Supergrupos Espinhaço e São Francisco, *in* Barbosa, J. S. F., M, M. J. F., Corrêa-Gomes, L. C., L, D. J. M., org., Geologia da Bahia. Pesquisa e Atualização de Dados, Vol. 2, Salvador, Companhia Baiana de Pesquisa Mineral - CBPM, p. 33–86.

Guimarães, J. T., Santos, R. A., Melo, R. C., 2008, Geologia da Chapada Diamantina Ocidental (Projeto Ibitiara-Rio de Contas): Série Arquivos Abertos 31, Companhia Baiana de Pesquisa Mineral - CBPM, Companhia Pesquisa de Recursos Minerais - CPRM.

Hansen, D. L., Nielsen, S. B., 2003, Why rifts invert in compression: Tectonophysics, v. 373, no. 1-4, p. 5–24, doi:10.1016/S0040-1951(03)00280-4.

Hossack, J. R., 1978, The correction of stratigraphic sections for tectonic finite strain in the Bygdin area, Norway: Journal of the Geological Society, v. 135, no. 2, p. 229–241, doi:10.1144/gsjgs.135.2.0229.

Judge, P. A., Allmendinger, R. W., 2011, Assessing uncertainties in balanced cross sections: Journal of Structural Geology, v. 33, no. 4, p. 458–467, doi:10.1016/j.jsg.2011.01.006.

Lacombe, O., Bellahsen, N., 2016, Thick-skinned tectonics and basement-involved fold–thrust belts: insights from selected Cenozoic orogens: Geological Magazine, v. 153, no. 5-6, p. 763–810, doi:10.1017/S0016756816000078.

Launeau, P., Cruden, A. R., 1998, Magmatic fabric acquisition mechanisms in a syenite: results of a combined anisotropy of magnetic susceptibility and image analysis study: Journal of Geophysical Research: Solid Earth, v. 103, no. B3, p. 5067–5089, doi:10.1029/97JB02670.

Launeau, P., Robin, P.-Y. F., 2005, Determination of fabric and strain ellipsoids from measured sectional ellipses—implementation and applications: Journal of Structural Geology, v. 27, no. 12, p. 2223–2233, doi:10.1016/j.jsg.2005.08.003.

Lingrey, S., Vidal-Royo, O., 2015, Evaluating the quality of bed length and area balance in 2D structural restorations: Interpretation, v. 3, no. 4, p. SAA133–SAA160, doi:10.1190/INT-2015-0126.1.

Loureiro, H. S. C., Bahiense, I. C., Neves, J. P., Guimarães, J. T., Teixeira, L. R., Santos, R. A., Melo, R. C., 2009, Geologia e recursos minerais da parte norte do corredor de deformação do Paramirim (Projeto Barra - Oliveira dos Brejinhos): Série Arquivos Abertos 33, Companhia Baiana de Pesquisa Mineral - CBPM.

Martins-Ferreira, M. A. C., 2019, Effects of initial rift inversion over fold-and-thrust development in a cratonic far-foreland setting: Tectonophysics, v. 757, p. 88–107, doi:10.1016/j.tecto.2019.03.009.

Mount, V. S., Suppe, J., Hook, S. C., 1990, A forward modeling strategy for balancing cross sections: AAPG bulletin, v. 74, no. 5, p. 521–531, doi:10.1306/0C9B235D-1710-11D7-8645000102C1865D.

Pedreira, A. J., Arcanjo, J. B., Pedrosa, C. J., Oliveira, J. E., Silva, B. C. E., 1975, Projeto Bahia; Geologia da Chapada Diamantina: Relatório Final. Salvador: CPRM, v. 1.

Pedrosa-Soares, A. C., Alkmim, F. F., 2011, How many rifting events preceded the development of the Araçuaí-West Congo orogen?: Geonomos, v. 19, p. 244–251, doi:10.18285/geonomos.v19i2.56.

Pedrosa-Soares, A. C., Alkmim, F. F., Tack, L., Noce, C. M., Babinski, M., Silva, L. C., Martins-Neto, M. A., 2008, Similarities and differences between the Brazilian and African counterparts of the Neoproterozoic Araçuaí-West Congo orogen: Geological Society, London, Special Publications, v. 294, no. 1, p. 153–172, doi:10.1144/SP294.9.

Pedrosa-Soares, A. C., Noce, C., Wiedemann, C., Pinto, C. P., 2001, The Araçuaı-West-Congo Orogen in Brazil: an overview of a confined orogen formed during Gondwanaland assembly: Precambrian research, v. 110, no. 1-4, p. 307–323.

Ramsay, J. G., 1967, Folding and fracturing of rocks: New York, McGraw-Hill, 568 p.

Ramsay, J. G., Wood, D. S., 1973, The geometric effects of volume change during deformation processes: Tectonophysics, v. 16, no. 3-4, p. 263–277.

Robin, P.-Y. F., 2002, Determination of fabric and strain ellipsoids from measured sectional ellipses—theory: Journal of Structural Geology, v. 24, no. 3, p. 531–544, doi:10.1016/S0191-8141(01)00081-5.

Sanderson, D. J., Marchini, W. R. D., 1984, Transpression: Journal of structural Geology, v. 6, no. 5, p. 449–458, doi:10.1016/0191-8141(84)90058-0.

Serra, J., 1982, Image analysis and mathematical morphology: London, Academic press, 610 p.

Suppe, J., 1983, Geometry and kinematics of fault-bend folding: American Journal of science, v. 283, no. 7, p. 684–721.

Süssenberger, A., Neves, B. B. d. B., Wemmer, K., 2014, Dating low-grade metamorphism and deformation of the Espinhaço Supergroup in the Chapada Diamantina (Bahia, NE Brazil): a K/Ar fine-fraction study: Brazilian Journal of Geology, v. 44, no. 2, p. 207–220, doi:10.5327/Z2317-4889201400020003.

Teixeira, L. R., 2005, Projeto Ibitiara-Rio de Contas: relatório temático de litogeoquímica: Salvador, Convênio CPRM/CBPM, 33 p.

Teixeira, W., Oliveira, E. P., Marques, L., 2017, Nature and Evolution of the Archean Crust of the São Francisco Craton, *in* Heilbron, M., Cordani, U. G., Alkmim, F. F., org., São Francisco Craton, Eastern Brazil: Tectonic Genealogy of a Miniature Continent, Springer, p. 34–61.

Trompette, R. R., Uhlein, A., Silva, M. E., Karmann, I., 1992*a*, O Cráton Brasiliano do São Francisco: uma revisão: Revista Brasileira de Geociências, v. 22, no. 4, p. 481–486.

Trompette, R., Uhlein, A., Silva, M. E., Karmann, I., 1992*b*, The Brasiliano São Francisco craton revisited (central Brazil): Journal of South American Earth Sciences, v. 6, no. 1-2, p. 49–57, doi:10.1016/0895-9811(92)90016-R.

Turpin, L., Maruejol, P., Cuney, M., 1988, U-Pb, Rb-Sr and Sm-Nd chronology of granitic basement, hydrothermal albitites and uranium mineralization (Lagoa Real, South-Bahia, Brazil): Contributions to Mineralogy and Petrology, v. 98, no. 2, p. 139–147, doi:10.1007/BF00402107.

Vidal-Royo, O., Hearon IV, T. E., Connors, C. D., Bland, S., Schaefer, F., Ferrer, O., Mora, A., de Vera, J., Guzofski, C. A., Rodríguez, F. et al., 2015, Introduction to special section: Balancing, restoration, and palinspastic reconstruction: Interpretation, v. 3, no. 4, p. SAAi–SAAiii, doi:10.1190/INT2015-0916-SPSEINTRO.1.

Vollmer, F. W., 2018, Automatic contouring of geologic fabric and finite strain data on the unit hyperboloid: Computers & Geosciences, v. 115, p. 134–142, doi:10.1016/j.cageo.2018.03.006.

Woodward, N. B., Gray, D. R., Spears, D. B., 1986, Including strain data in balanced cross-sections: Journal of Structural Geology, v. 8, no. 3-4, p. 313–324, doi:10.1016/0191-8141(86)90052-0.

8 APPENDIX

8.1 Sample Field Data

This section presents field data from outcrops where the samples used in this presented work were collected. All data is shown in Table 2.

Table 2: Attitude geological data from the sample outcrops. Both bedding and foliation are represented using the Right Hand Rule (RHR) convention, whereas lineation data follows the trend/plunge system.

Sample Code	Location		Map Unit	Lithology	Attitude Data		
	Longitude	Latitude			Sedimentary Bedding	Foliation	Intersect Lineation
CD-01B	41º 40' 09.2" S	13º 16' 11.7" W	Gavião Complex	Orthogneisse	-	352/85	-
CD-03A	41º 35' 33.3" S	13º 16' 11.7" W	Novo Horizonte Fm.	Meta-sandstone	-	355/80	-
CD-06A	41º 43' 05.1" S	13º 16' 36.0" W	Ouricuri do Ouro Fm.	Meta-sandstone	165/86	-	-
CD-11	41º 56' 12.5" S	13º 05' 21.6" W	Açuruá Fm.	Meta-sandstone	336/33	150/35	336/01
CD-16	42º 02' 13.4" S	13º 06' 54.6" W	Ouricuri do Ouro Fm.	Meta-siltstone	323/14	167/75	350/06
CD-23	42º 00' 58.9" S	13º 18' 41.4" W	Açuruá Fm.	Meta-sandstone	019/25	118/86	127/20
CD-28	42º 03' 37.5" S	13º 25' 30.8" W	Açuruá Fm.	Meta-sandstone	148/20	338/67	150/05
CD-30A	42º 03' 28.3" S	13º 25' 15.6" W	Ouricuri do Ouro Fm.	Meta-sandstone	308/25	149/75	321/07
CD-40	42º 12' 55.5" S	13º 26' 13.7" W	Serra da Gameleira Fm.	Meta-sandstone	-	-	-

8.2 2D and 3D Strain Data

For the supplementary data of 2D strain analysis, we present the Shape Preferred Orientation ellipses of each sample obtained by the Inertia Tensor method (Launeau and Cruden, 1998). Later, all ellipses were used to compute the best fit ellipsoid using the using the software *ELLIPSOID* (Robin, 2002; Launeau and Robin, 2005). Finally, Table 3 summarizes the 2D strain data obtained for all samples used in this study followed by all microphotographs and computed shape preferred ellipses for all samples.

Table 3: Two Dimensional (2D) Strain Data - Shape preferred orientation ellipses for all planes used to compute best fit ellipsoids.

	AC Plane				AB Plane				BC Plane			
Sample Code	n	R_s	ϕ (°)	Strike/Dip	n	R_s	ϕ (°)	Strike/Dip	n	R_s	ϕ (°)	Strike/Dip
CD-01B	89	1.675	080.03	090/34	69	1.164	112.03	348/84	120	1.448	100.2	254/56
CD-03A	176	1.650	029.02	266/05	121	1.260	53.04	359/89	152	1.459	60.04	091/88
CD-06A	211	1.408	178.00	354/49	135	1.022	146.91	176/35	202	1.492	134.64	078/89
CD-11	237	1.350	037.47	240/80	208	1.088	132.39	159/41	176	1.214	175.4	344/48
CD-16	82	1.915	141.63	018/15	156	1.346	96.47	174/80	99	2.207	73.34	272/86
CD-23	164	1.219	123.67	242/04	405	1.218	128.14	318/88	364	1.125	112.37	046/86
CD-28	184	1.143	087.46	034/74	245	1.103	67.17	274/24	236	1.067	53.57	130/70
CD-30A	209	1.248	070.19	231/62	200	1.155	98.53	041/35	198	1.052	15.94	138/85
CD-40	150	1.146	043.03	143/82	164	1.117	131.93	237/55	158	1.133	110.67	039/40

* n is the number of quartz grains analyzed in each thin section to compute the Shape Preferred Orientation ellipse.
** Strike and Dip attitude follows the right hand rule convention (RHR) and represents the orientation of the thin section.

CD-01B

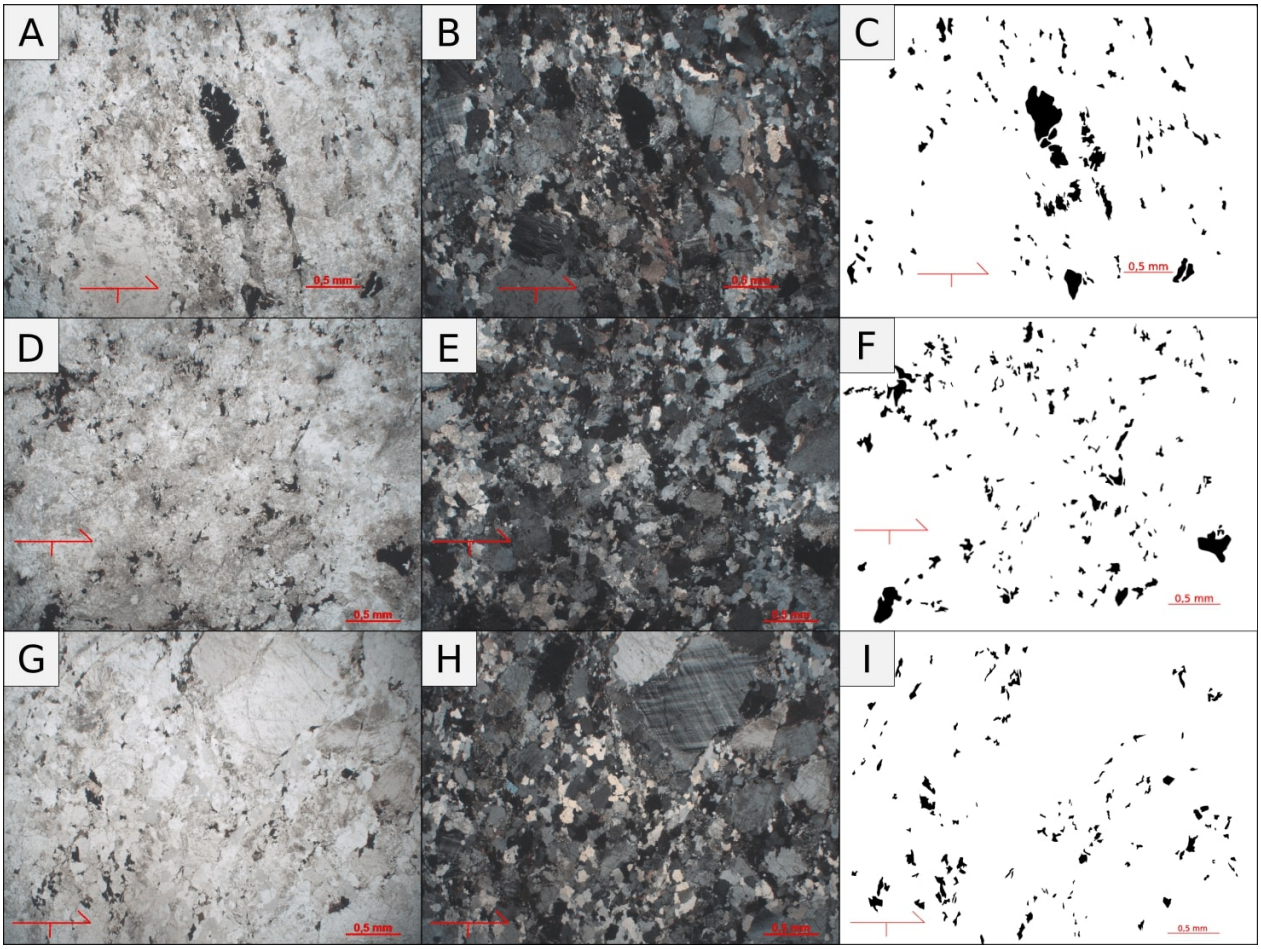

Figure 12: A,D,G: Polarized light microphotograph of the thin sections of planes AC, AB and BC of sample CD-01B, respectively. **B, E, H:** Cross-Polarized light microphotograph of the thin sections of planes AC, AB and BC from sample CD-01B, respectively. **C, F, I:** Single quartz grain digitized for SPO analysis of planes AC, AB and BC from sample CD-01B.

Sample CD-01B is a high grade metamorphic rock, composed basically by quartz, plagioclase and K-feldspar from the Gavião Complex. For this sample, opaque minerals, mainly ilmenite, were analyzed as strain markers. Sections AC and BC presented moderate to high shape ratios (R), while section AB, obtained a lower R, close to 1 (Figure 13). Thin sections microphotographs used to calculate the SPO are displayed in Fig. 12. The parameters of the best-fit ellipsoid can be seen in Fig. 14.

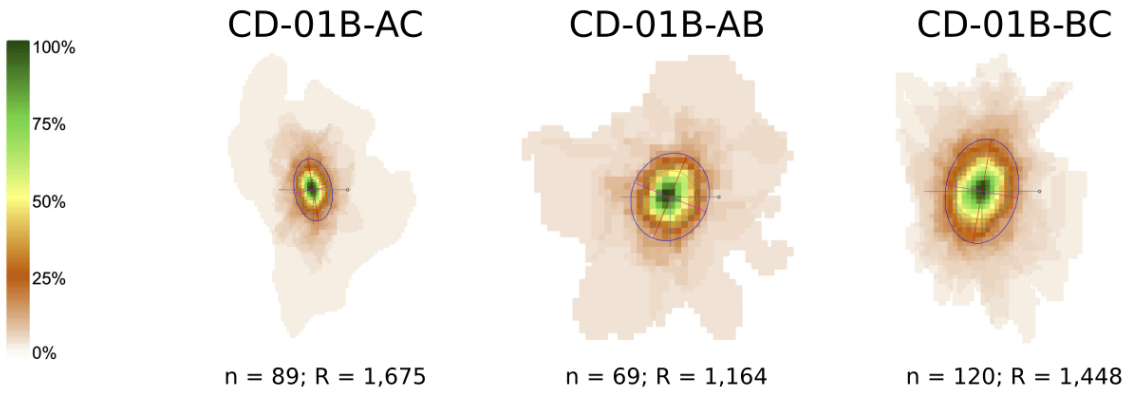

Figure 13: Shape preferred orientation ellipse of Sample CD-01B.

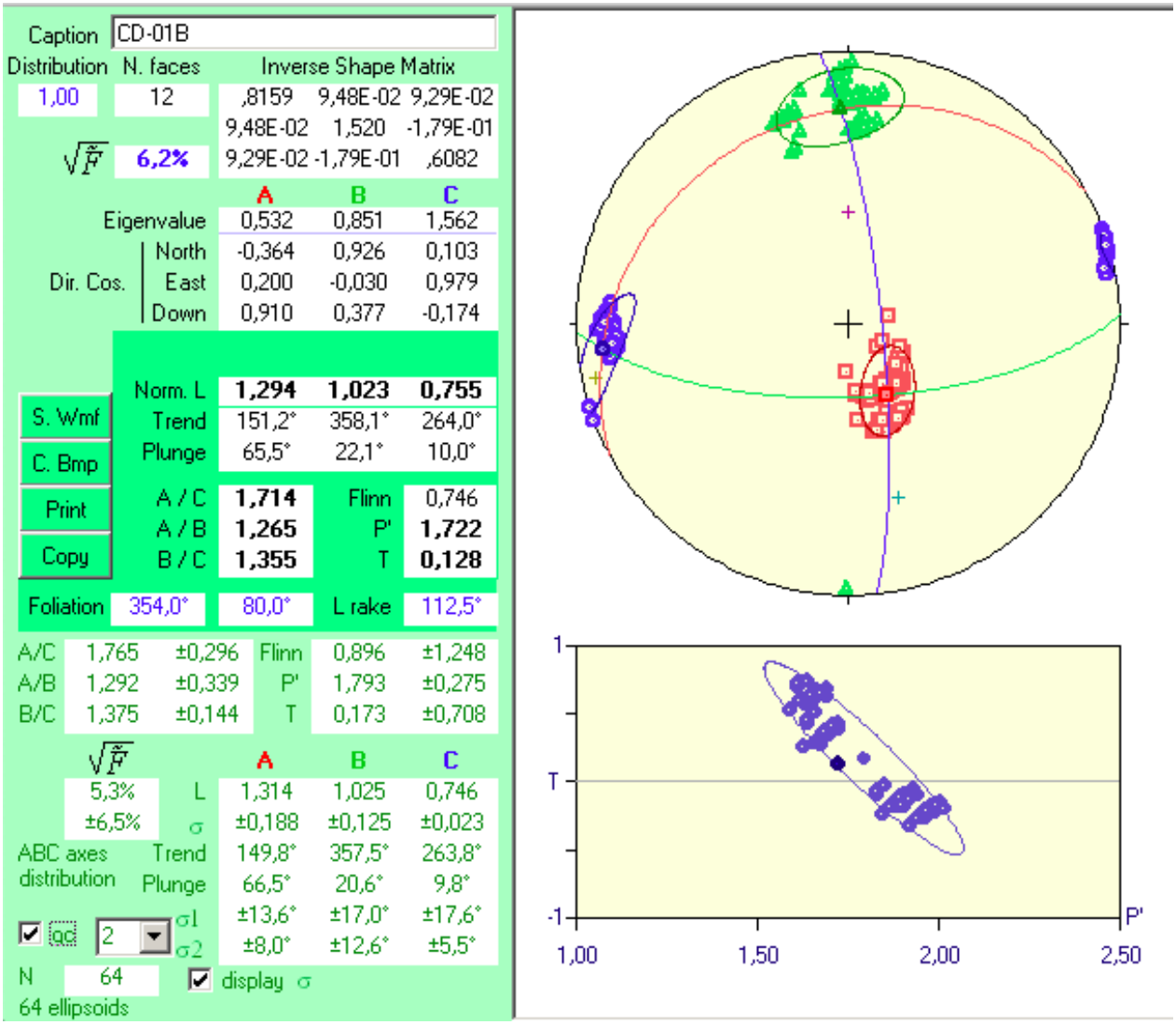

Figure 14: Best-fit ellipsoid parameters from Sample CD-01B. Results direct from the program ELLIPSOID screen.

CD-03A

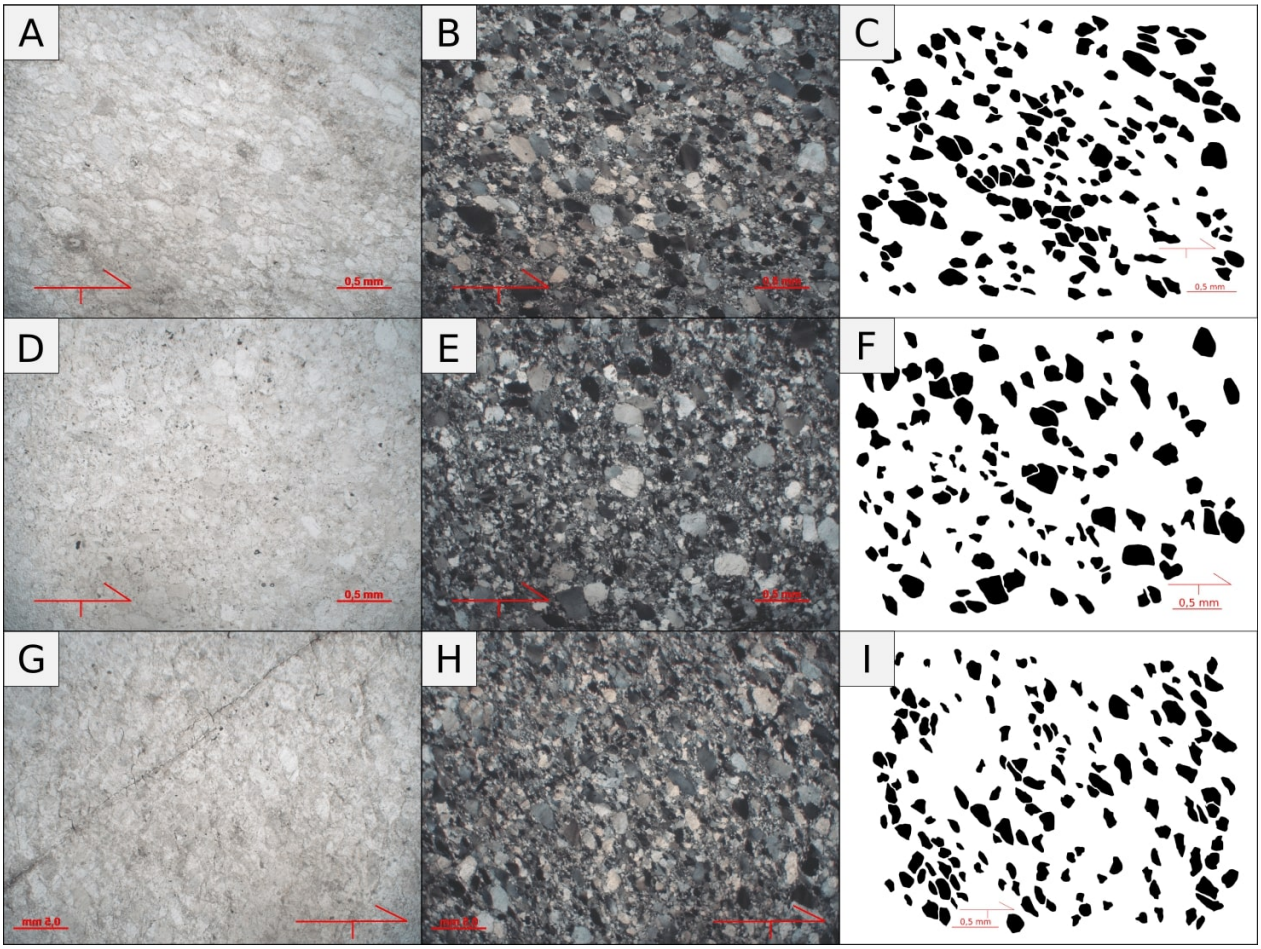

Figure 15: A,D,G: Polarized light microphotograph of the thin sections of planes AC, AB and BC of sample CD-03A, respectively. **B, E, H:** Cross-Polarized light microphotograph of the thin sections of planes AC, AB and BC from sample CD-03A, respectively. **C, F, I:** Single quartz grain digitized for SPO analysis of planes AC, AB and BC from sample CD-03A.

The CD-03A sample is an extremely foliated metarenite, with deformation of detritic quartz grains subordinated to the main foliation from the Novo Horizonte Formation. This sample lies close to the contact between the Basement and the above mentioned Formation, marked by major thrust faults. Sections present low to intermediate shape ratio values, ranging from 1.2 to 1.4 (Figure 16). The thin sections microphotographs used to calculate the SPO are displayed in Fig. 15. The parameters of the best-fit ellipsoid can be seen in Fig. 17.

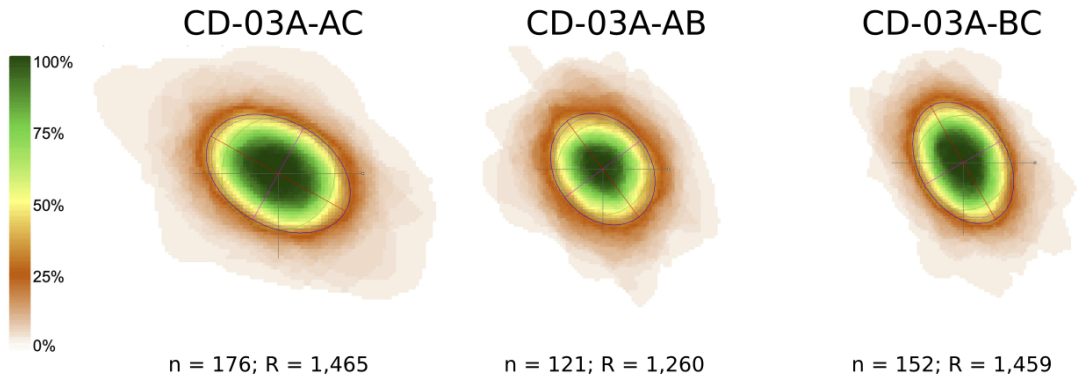

Figure 16: Shape preferred orientation ellipse of sample CD-03A.

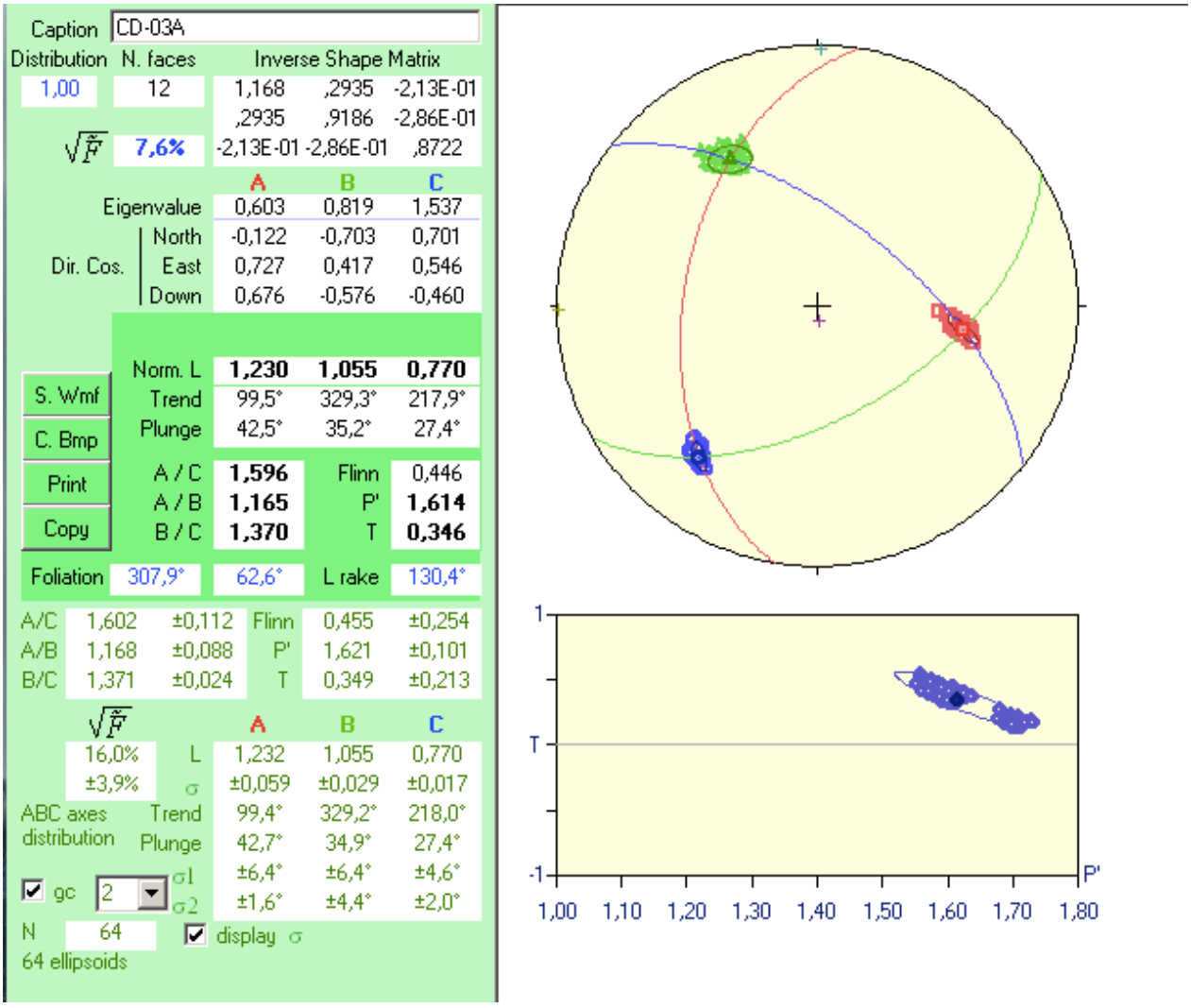

Figure 17: Best-fit ellipsoid parameters from Sample CD-03A. Results direct from the program ELLIPSOID screen.

CD-06A

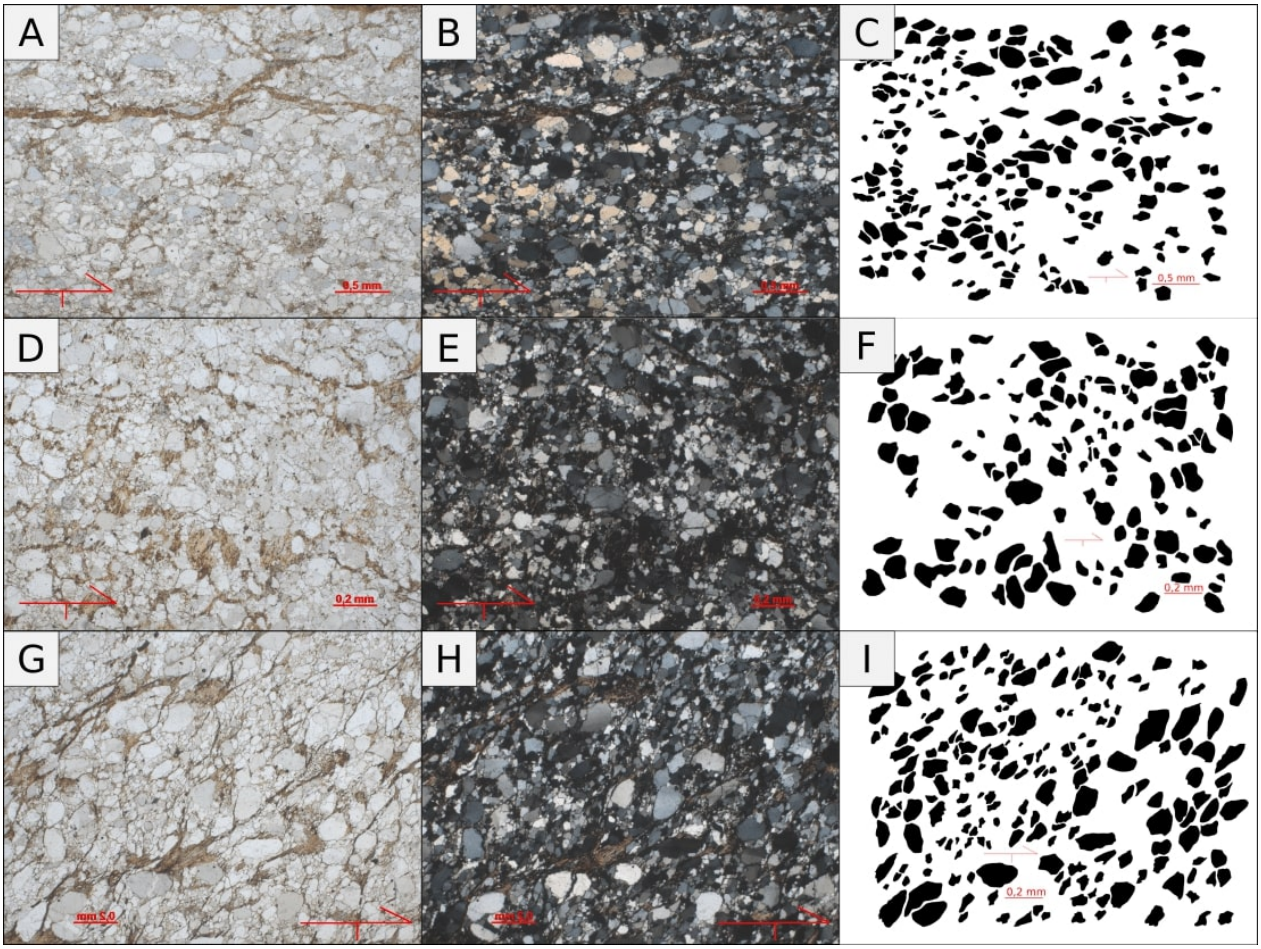

Figure 18: A,D,G: Polarized light microphotograph of the thin sections of planes AC, AB and BC of sample CD-06A, respectively. **B, E, H:** Cross-Polarized light microphotograph of the thin sections of planes AC, AB and BC from sample CD-06A, respectively. **C, F, I:** Single quartz grain digitized for SPO analysis of planes AC, AB and BC from sample CD-06A.

The CD-06A sample is a poorly sorted impure metarenite, from the Ouricuri do Ouro, with sub-angular to sub-round quartz grains, oriented preferably, parallel to the preferred slaty cleavage. As well as CD-03A, sample CD-06A lies close to the contact between the Basement and the above mentioned Formation, marked by major thrust faults. Sections AC and BC have a moderate shape ratio ranging from 1.4 to 1.5, while section AB has a low R, equals to 1.02 (Figure 19). Thin sections microphotographs used to calculate the SPO are displayed in Fig. 18. The parameters of the best-fit ellipsoid can be seen in Fig. 20.

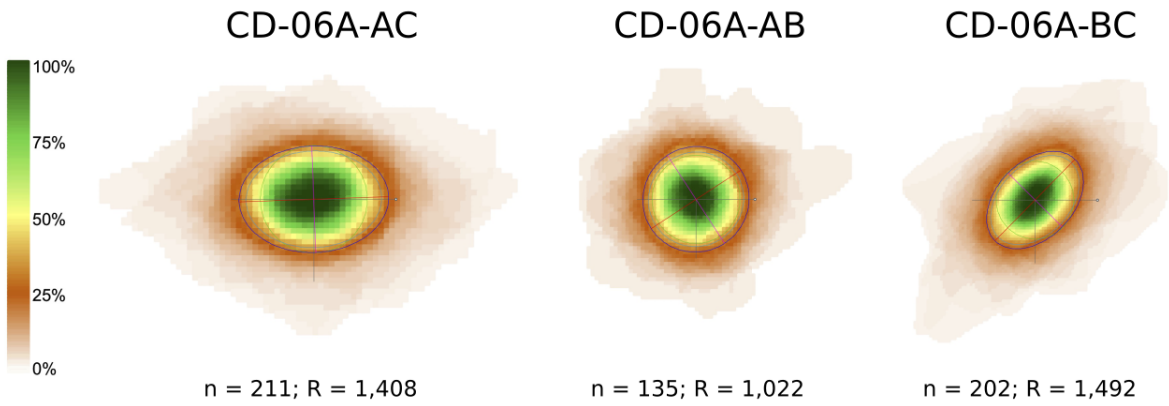

Figure 19: Shape preferred orientation ellipses of sample CD-06A.

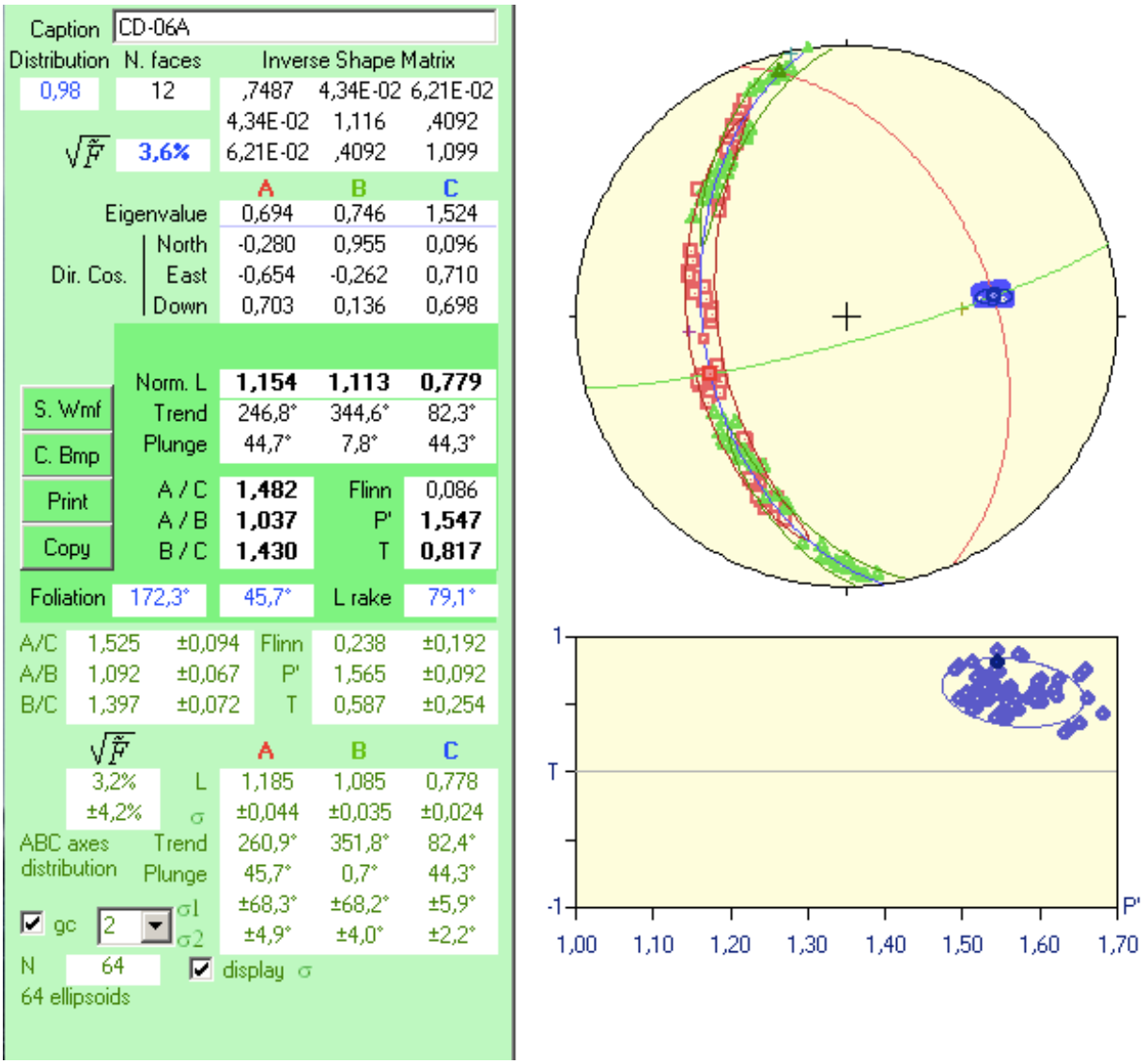

Figure 20: Best-fit ellipsoid parameters from Sample CD-06A. Results direct from the program ELLIPSOID screen.

CD-11

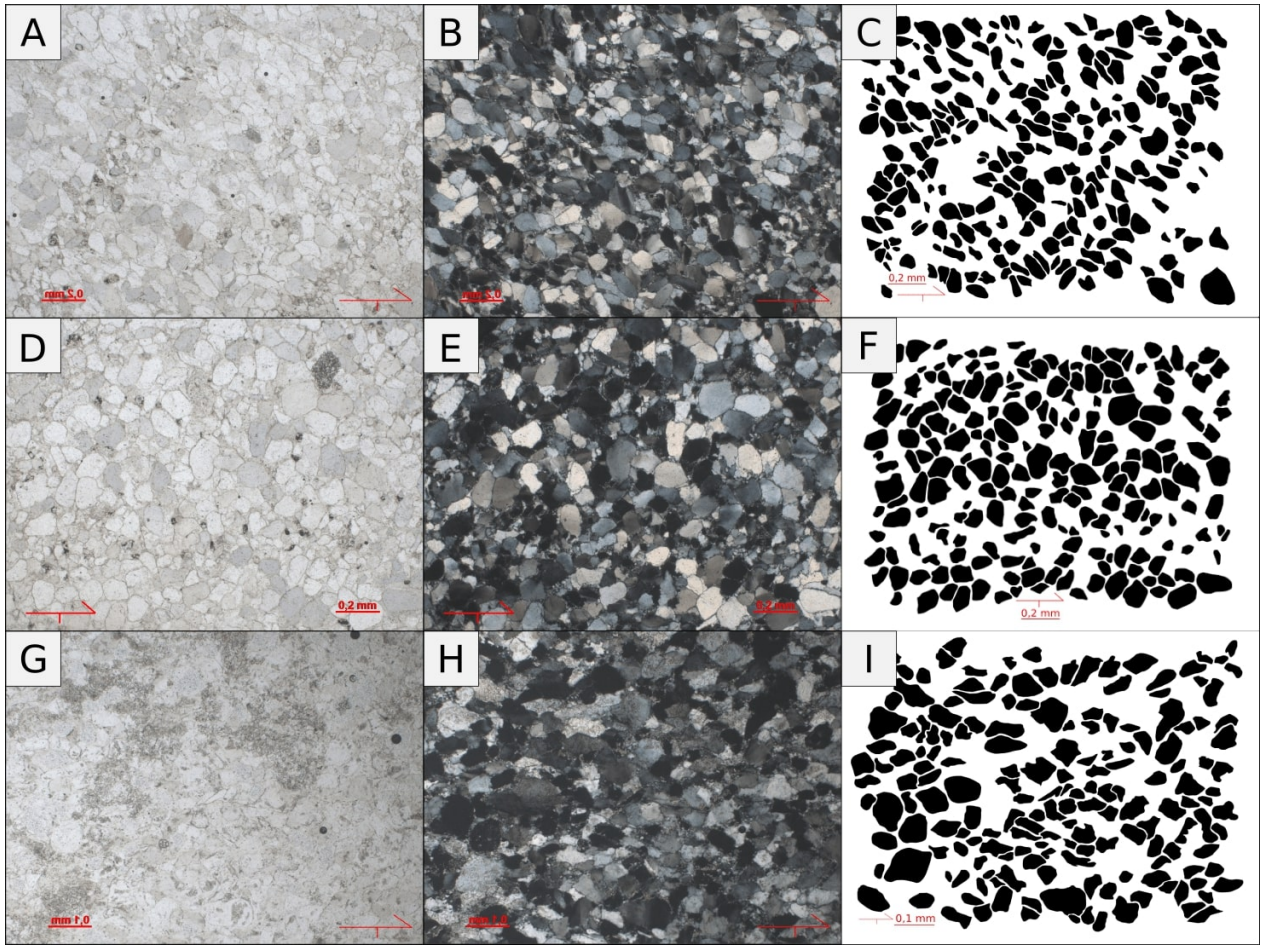

Figure 21: A,D,G: Polarized light microphotograph of the thin sections of planes AC, AB and BC of sample CD-11, respectively. **B, E, H:** Cross-Polarized light microphotograph of the thin sections of planes AC, AB and BC from sample CD-11, respectively. **C, F, I:** Single quartz grain digitized for SPO analysis of planes AC, AB and BC from sample CD-11.

The CD-11 sample is a well sorted metarenite, with sub-angular to sub-rounded quartz grains, from the Açuruá Formation. The sample is at the western limb of the Piatã Brachysincline, in the northern part of this major structure. Slaty cleavage is well marked and in section A, bedding is preserved and arranged perpendicularly to the cleavage. Sections AC and BC, present low to intermediate shape ratios, between 1.2 and 1.35, while section AB, presents a R close to 1.0 (Figure 22). Thin sections microphotographs used to calculate the SPO are displayed in Fig. 21. The parameters of the best-fit ellipsoid can be seen in Fig. 23.

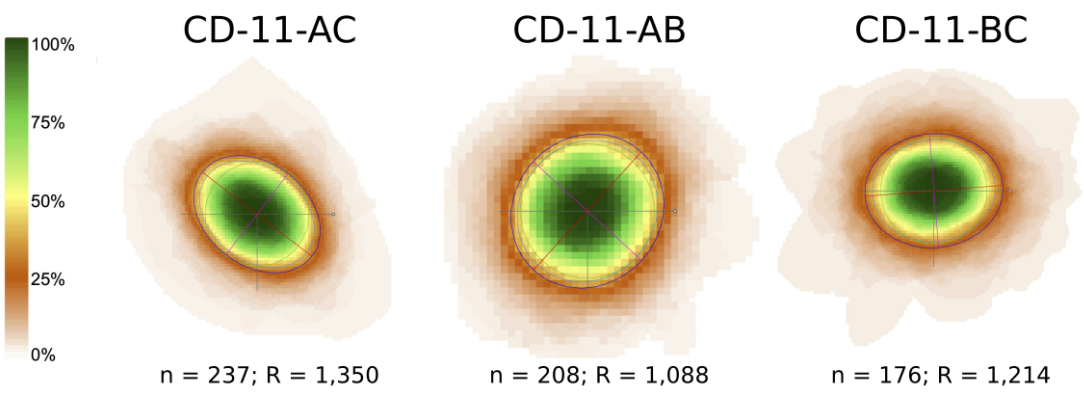

Figure 22: Shape preferred orientation ellipse of sample CD-11.

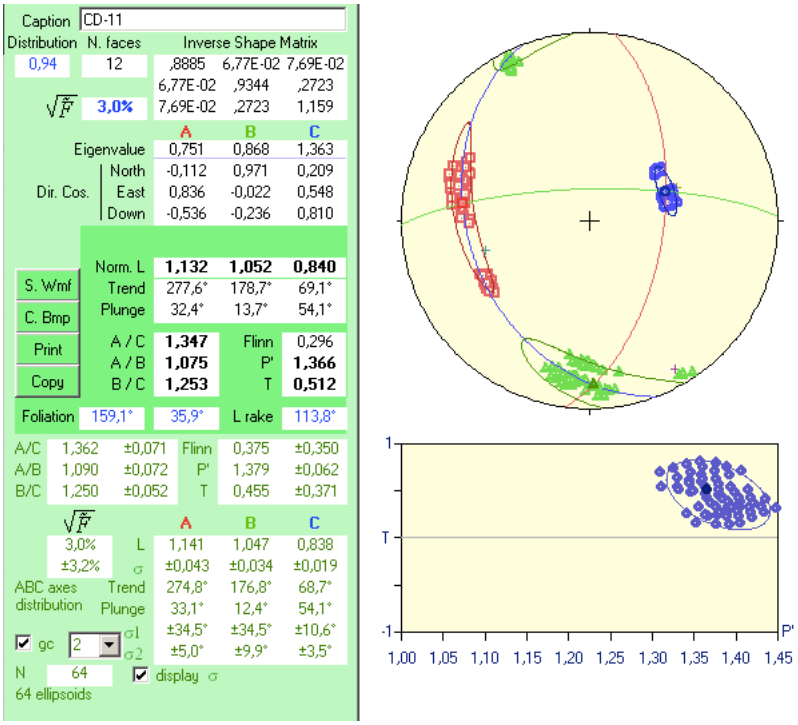

Figure 23: Best-fit ellipsoid parameters from Sample CD-11. Results direct from the program ELLIPSOID screen.

CD-16

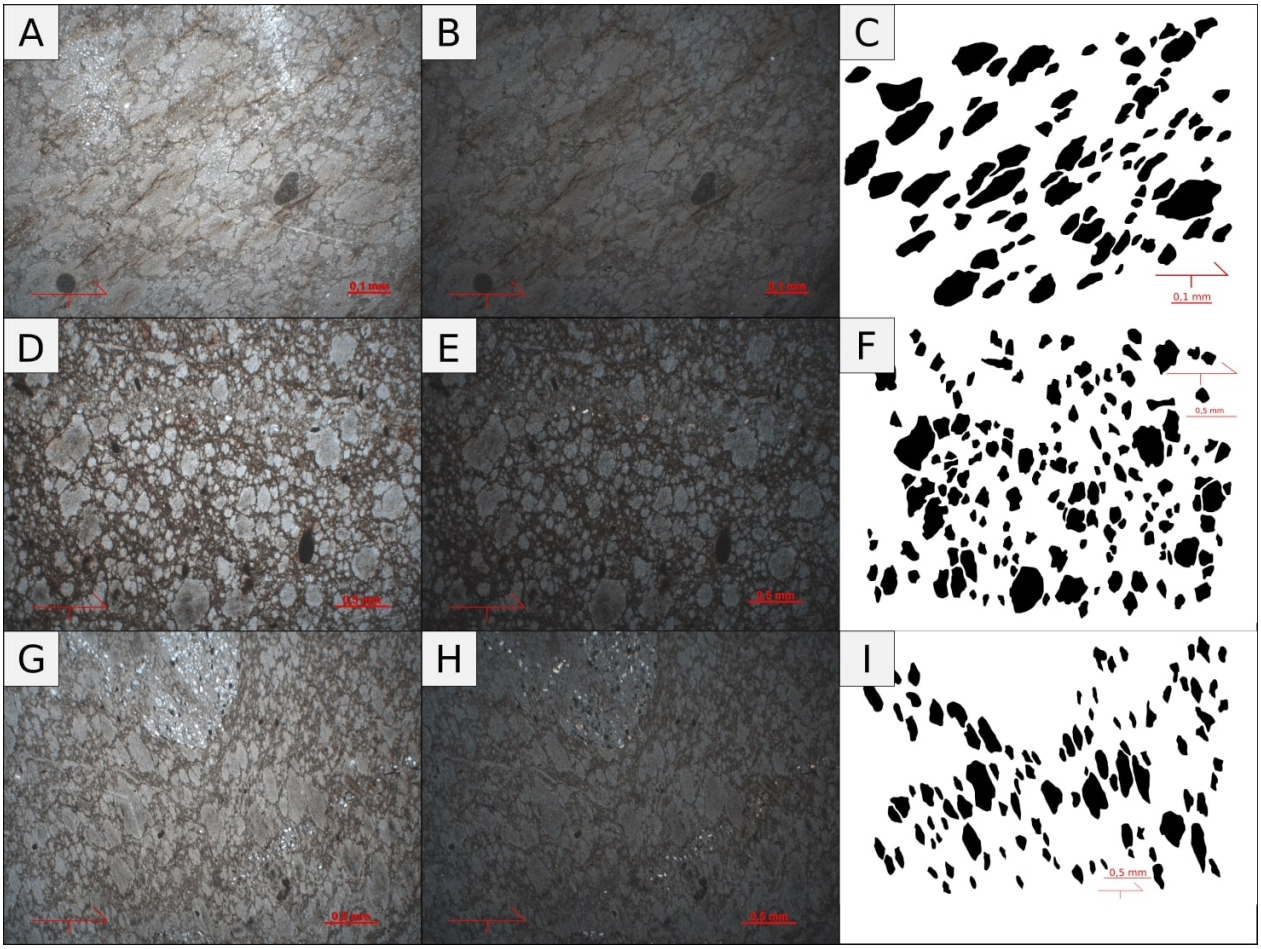

Figure 24: A,D,G: Polarized light microphotograph of the thin sections of planes AC, AB and BC of sample CD-16, respectively. **B, E, H:** Cross-Polarized light microphotograph of the thin sections of planes AC, AB and BC from sample CD-16, respectively. **C, F, I:** Single quartz grain digitized for SPO analysis of planes AC, AB and BC from sample CD-16.

The CD-16 sample is a very fine metasiltite, with a very well-defined slaty cleavage, from the Ouricuri do Ouro Formation lyng close to the axial plane trace of an anticline. For this sample, mud pellets were used as strain markers and, therefore, the rock's competence must be taken into account when evaluating the calculated deformation intensity. Sections AB and BC have a very high strain ratio, ranging from 1.9–2.2, while AB has a moderate R equals to 1.346 (Figure 25). Thin sections microphotographs used to calculate the SPO are displayed in Fig. 24. The parameters of the best-fit ellipsoid can be seen in Fig.26.

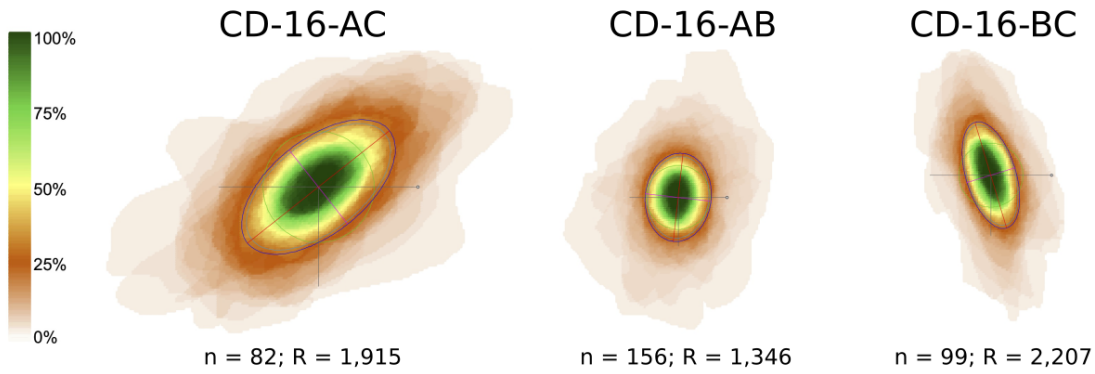

Figure 25: Shape preferred orientation ellipse of sample CD-16.

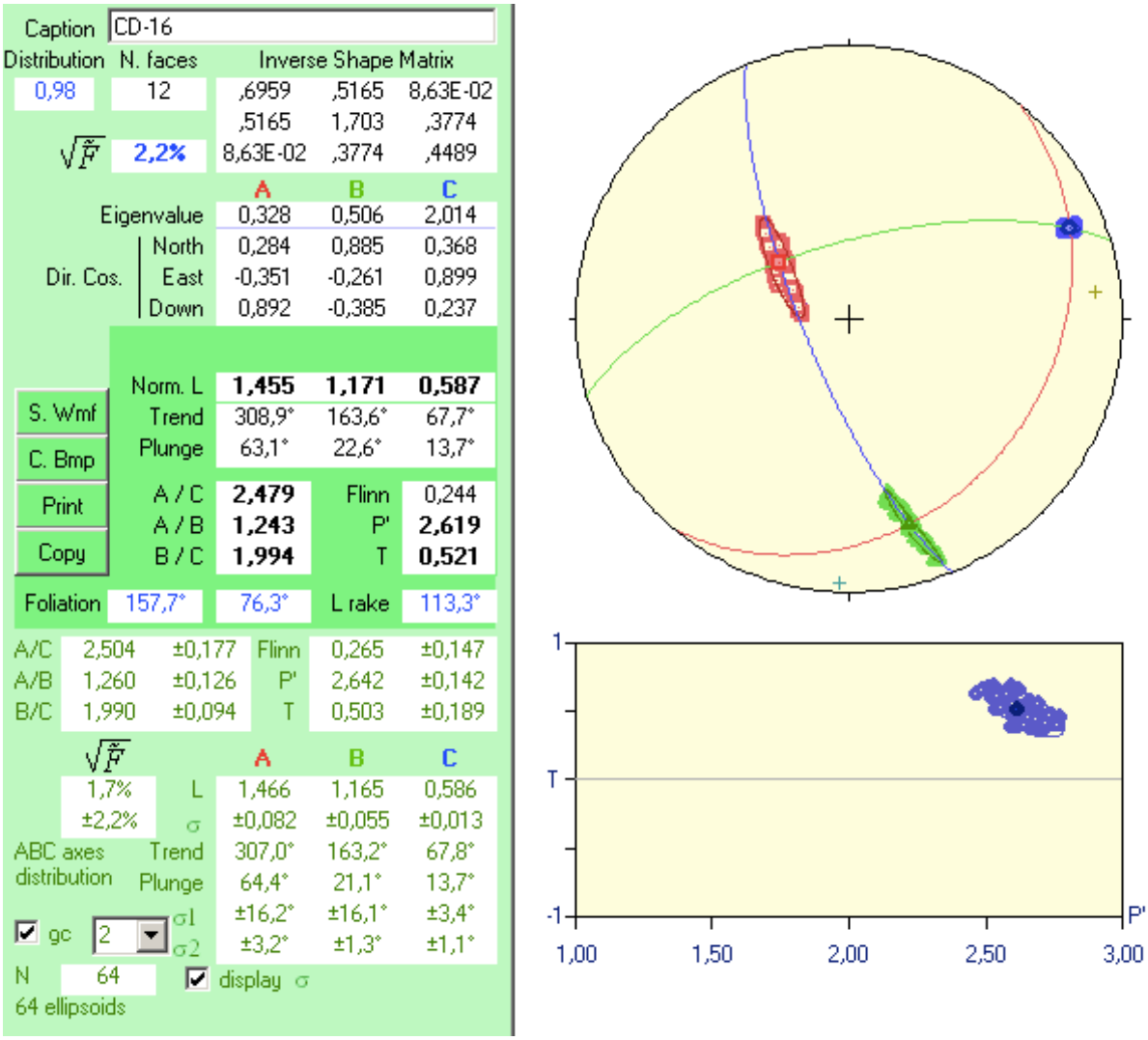

Figure 26: Best-fit ellipsoid parameters from Sample CD-16. Results direct from the program ELLIPSOID screen.

CD-23

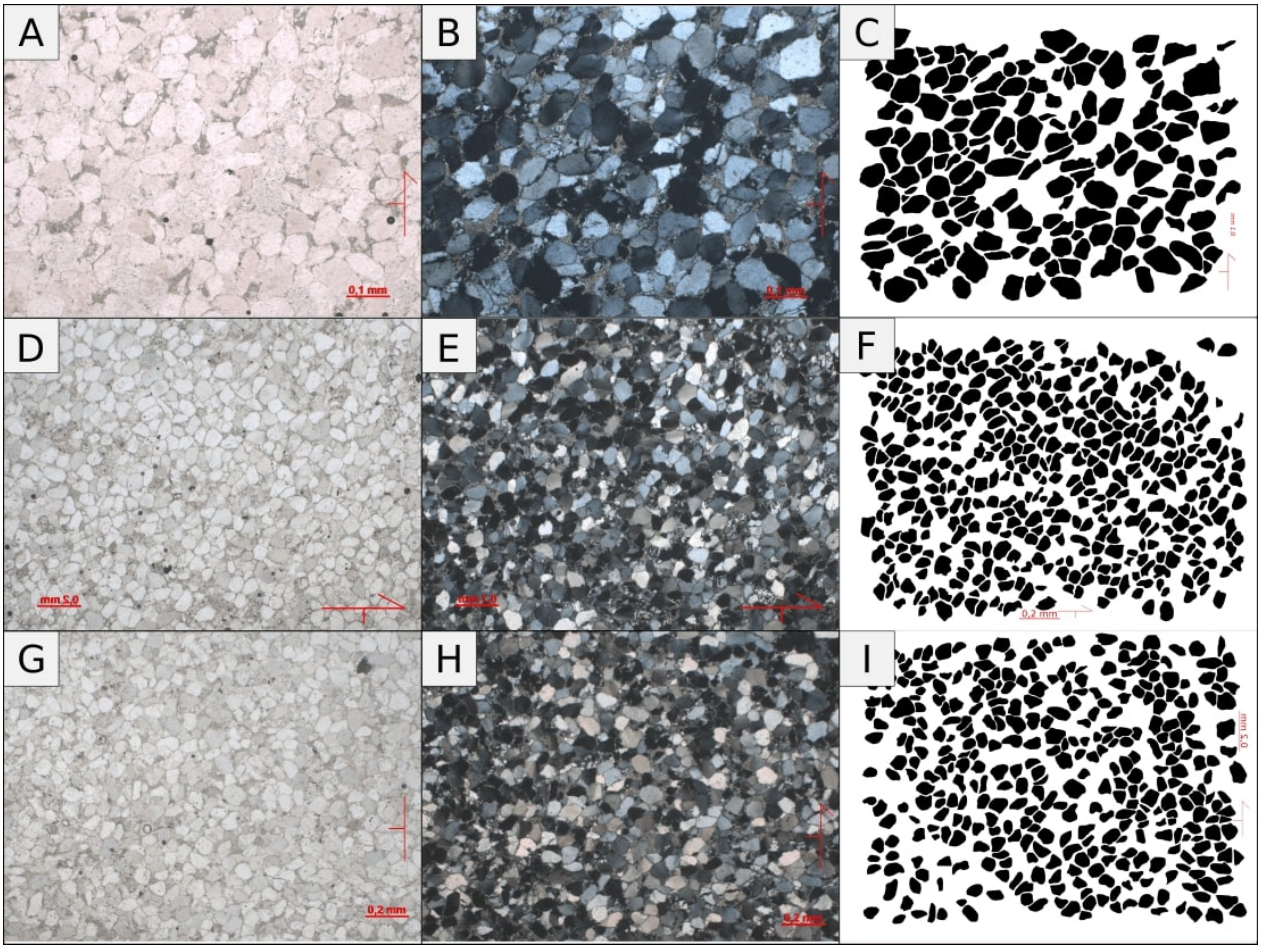

Figure 27: A,D,G: Polarized light microphotograph of the thin sections of planes AC, AB and BC of sample CD-23, respectively. **B, E, H:** Cross-Polarized light microphotograph of the thin sections of planes AC, AB and BC from sample CD-23, respectively. **C, F, I:** Single quartz grain digitized for SPO analysis of planes AC, AB and BC from sample CD-23.

The CD-23 sample is a fine, well sorted metarenite, with sub-angular to sub-rounded single quartz grains, from the Açuruá Formation. It lies close to the axial plane trace of a major syncline in the central portion of the study area. For this sample, more than 900 grains were processed, and all sections yielded low shape ratios, ranging from 1.1 to 1.2 (Figure 28). Thin sections microphotographs used to calculate the SPO are displayed in Fig. 27. The parameters of the best-fit ellipsoid can be seen in Fig. 29.

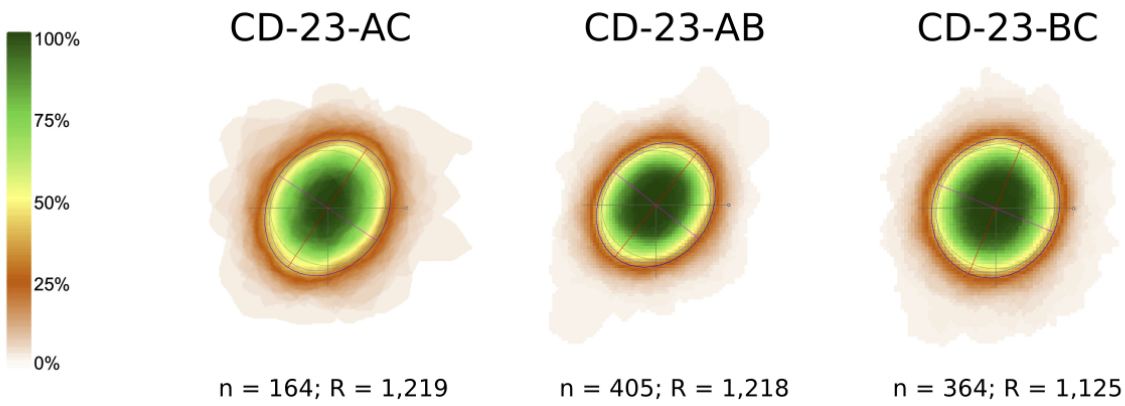

Figure 28: Shape preferred orientation ellipse of sample CD-23.

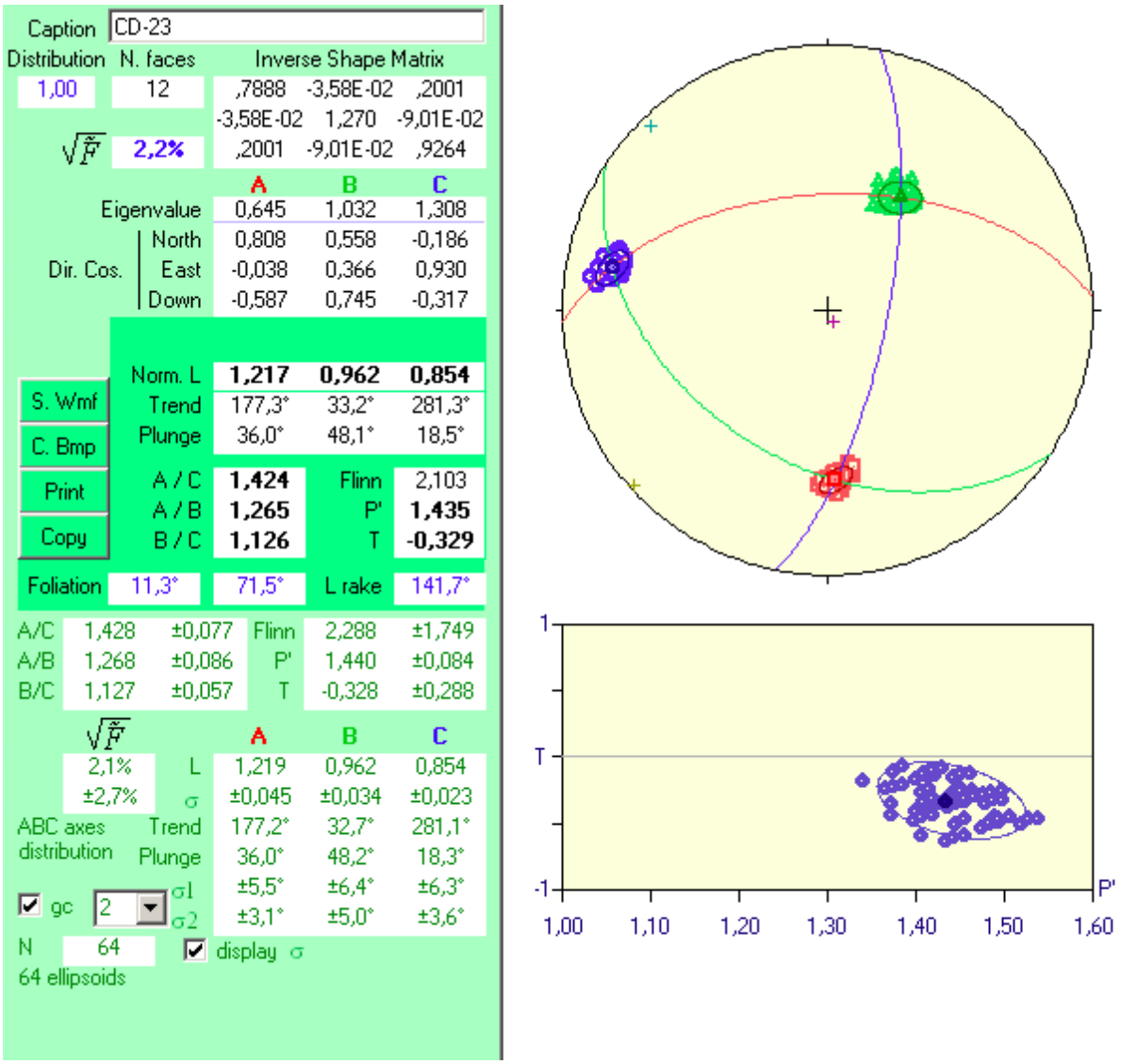

Figure 29: Best-fit ellipsoid parameters from Sample CD-23. Results direct from the program ELLIPSOID screen.

CD-28

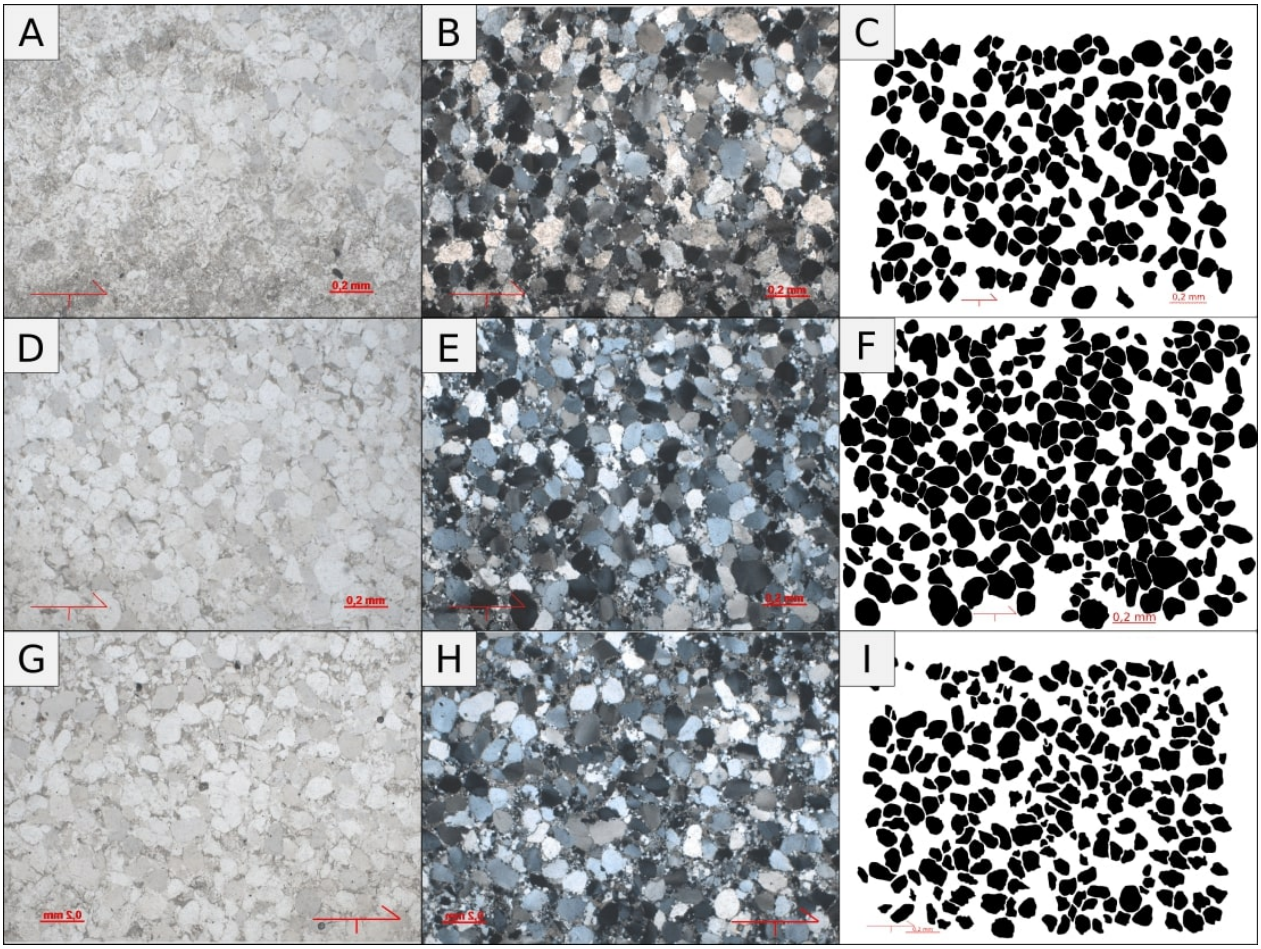

Figure 30: A,D,G: Polarized light microphotograph of the thin sections of planes AC, AB and BC of sample CD-28, respectively. **B, E, H:** Cross-Polarized light microphotograph of the thin sections of planes AC, AB and BC from sample CD-28, respectively. **C, F, I:** Single quartz grain digitized for SPO analysis of planes AC, AB and BC from sample CD-28.

The CD-28 sample is a fine, well sorted, mature quartz-metarenite from the Açuruá Formation in the southwestern region of the study area. It lies at the eastern limb of the Érico Cardoso inverted brachysincline, close to the geological contact defined by a thrust fault, separating a minor anticline structure to east and the fold structure mentioned above. All the analyzed sections yielded low shape ratio ranging from 1.07 to 1.14 (Figure 31). Thin sections microphotographs used to calculate the SPO are displayed in Fig. 30. The parameters of the best-fit ellipsoid can be seen in Fig.29.

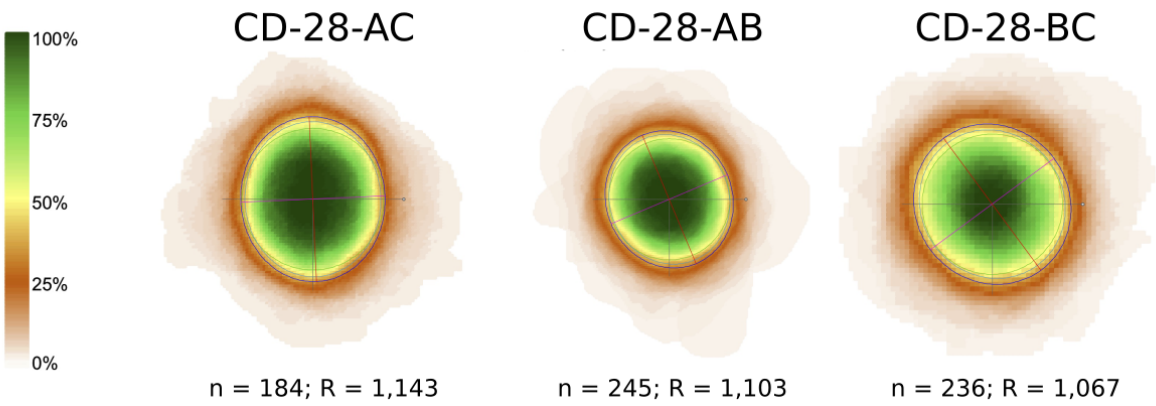

Figure 31: Shape preferrred orientation ellipses of sample CD-28.

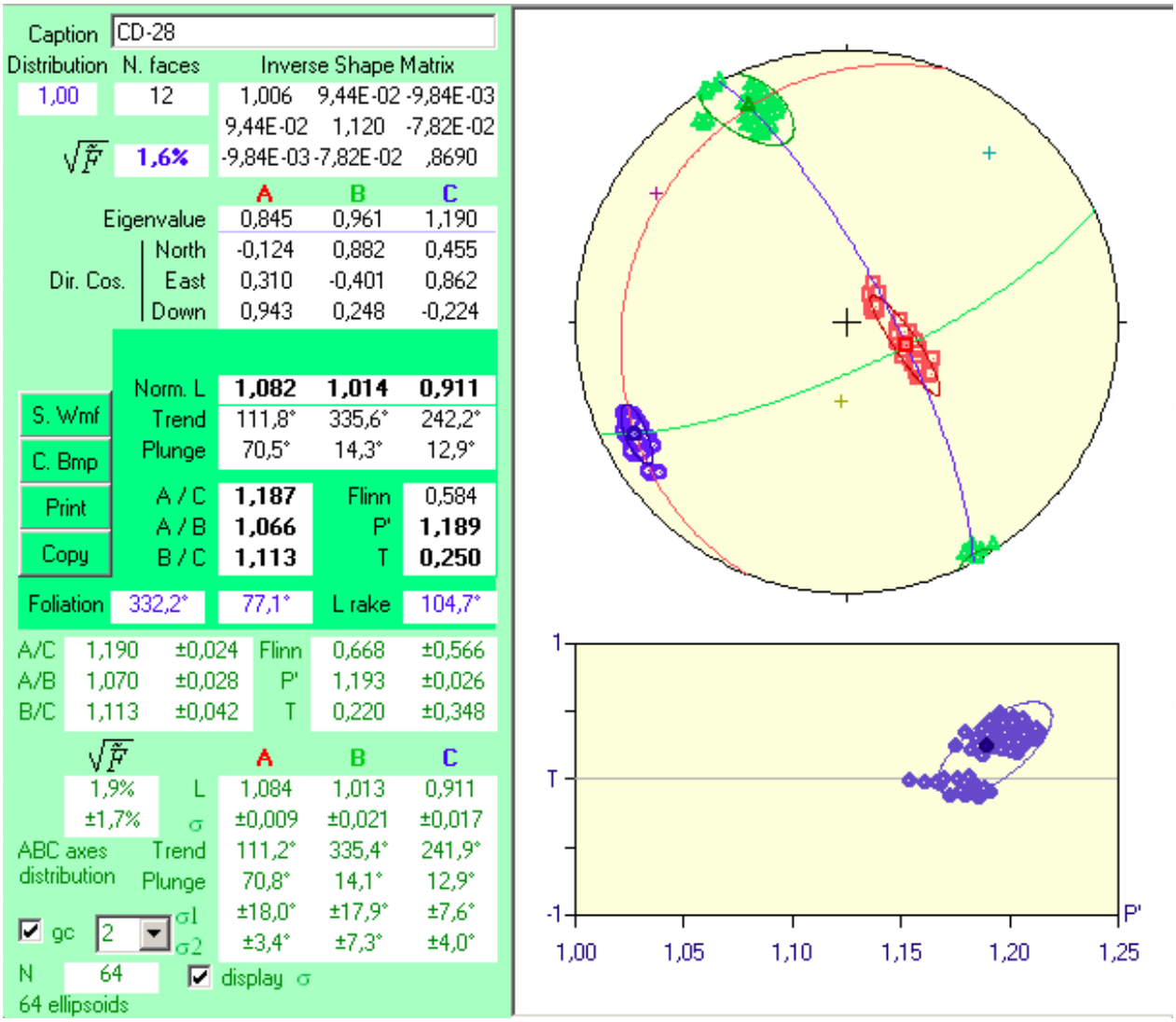

Figure 32: Best-fit ellipsoid parameters from Sample CD-28. Results direct from the program ELLIPSOID screen.

CD-30A

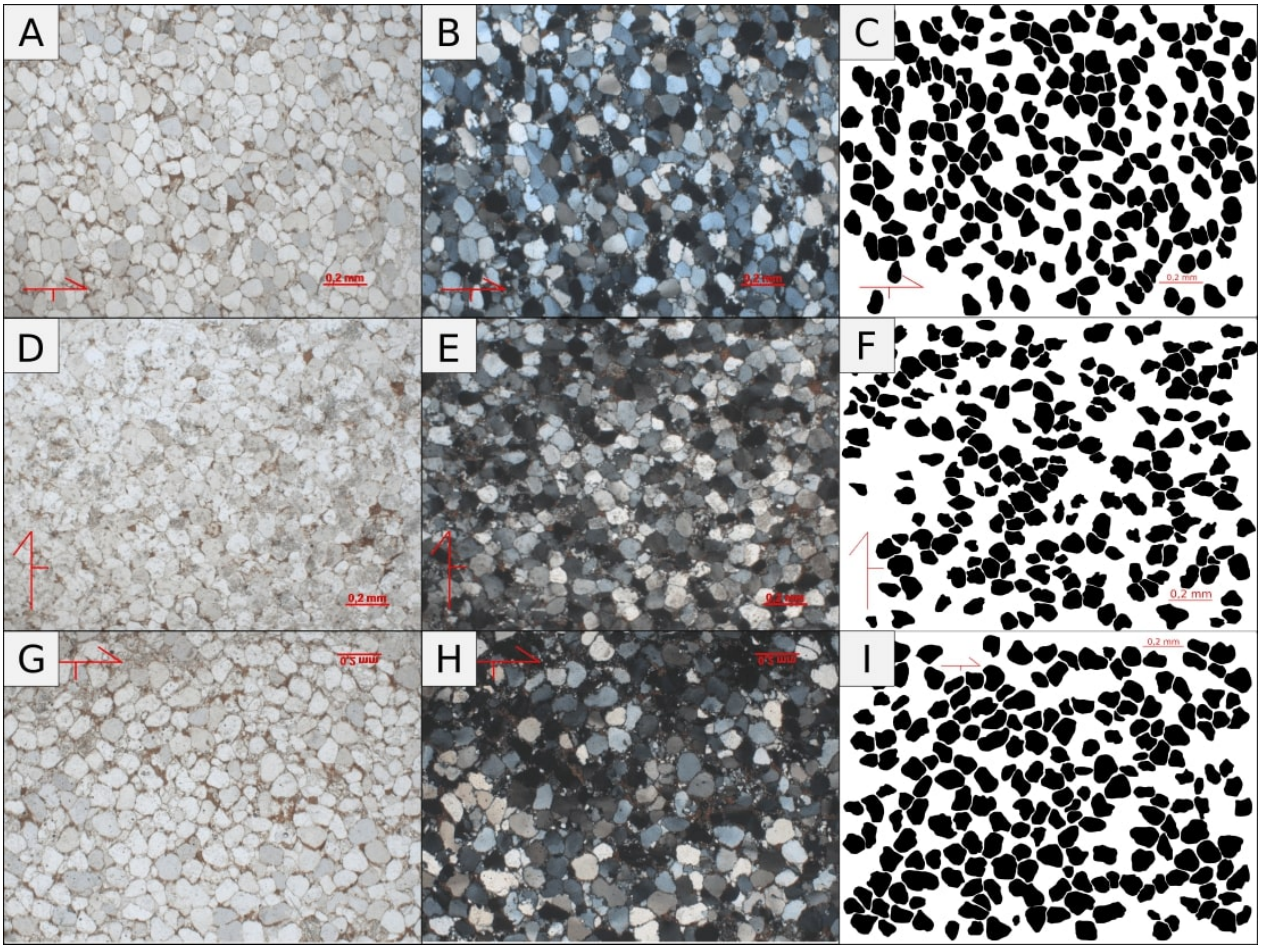

Figure 33: A,D,G: Polarized light microphotograph of the thin sections of planes AC, AB and BC of sample CD-30A, respectively. **B, E, H:** Cross-Polarized light microphotograph of the thin sections of planes AC, AB and BC from sample CD-30A, respectively. **C, F, I:** Single quartz grain digitized for SPO analysis of planes AC, AB and BC from sample CD-30A.

The CD-30A sample is a fine, well sorted quartz-metarenite from the Ouricuri do Ouro Formation. Just like CD-28, this sample lies close to a tectonic geological contact defined by a major thrust fault. More than 600 quartz grains were analyzed, with sections AB and BC showing low shape ratios values, between 1.05 and 1.15, while section AC presents an intermediate R, close to 1.25 (Figure 34). Thin sections microphotographs used to calculate the SPO are displayed in Fig. 33. The parameters of the best-fit ellipsoid can be seen in Fig.35.

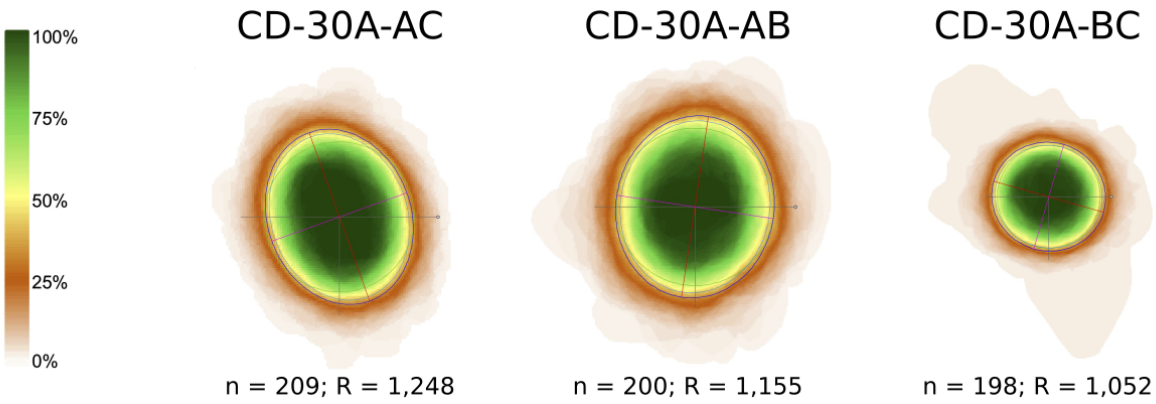

Figure 34: Shape preferred orientation ellipses from sample CD-30A.

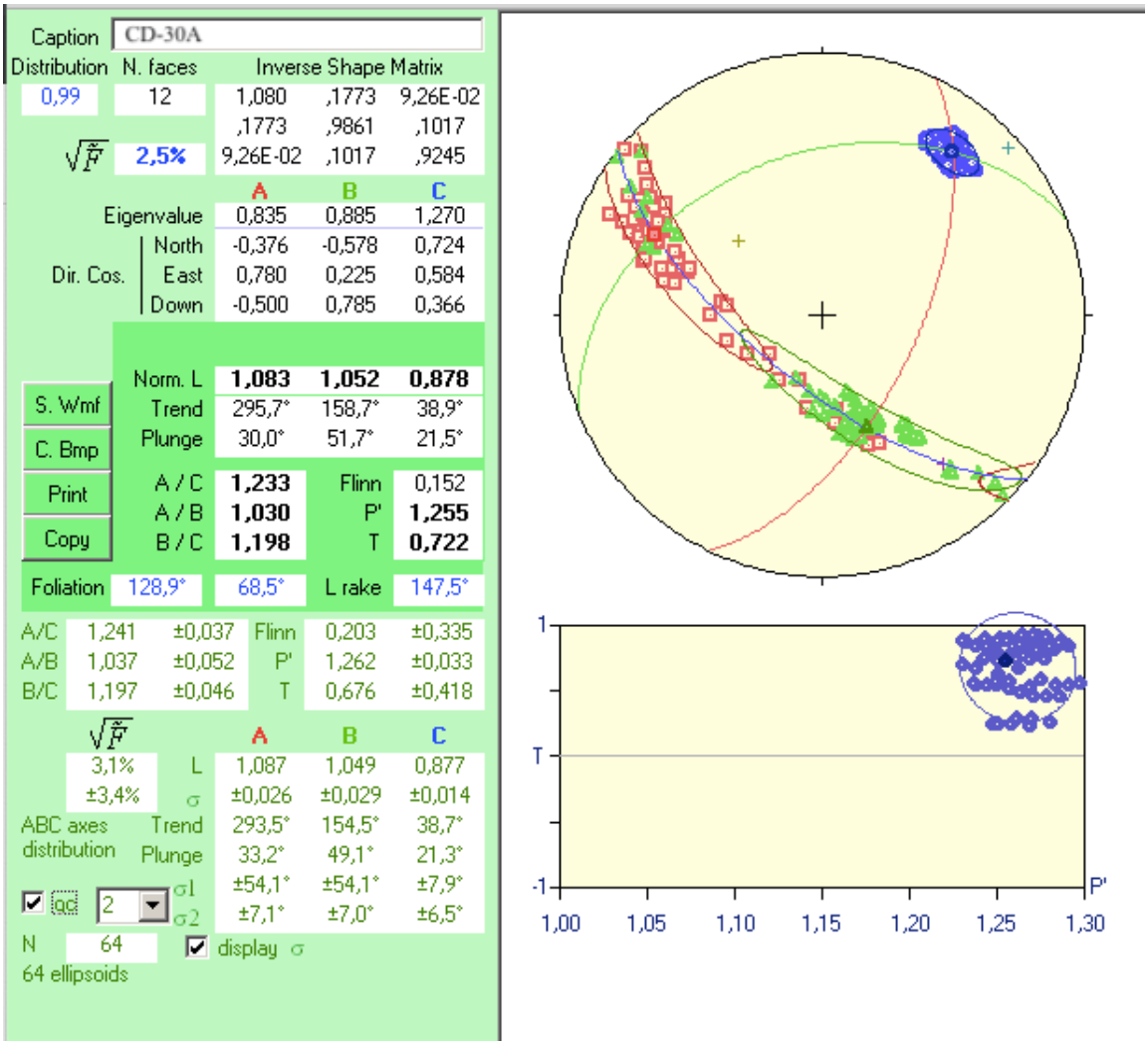

Figure 35: Best-fit ellipsoid parameters from Sample CD-30A. Results direct from the program ELLIPSOID screen.

CD-40

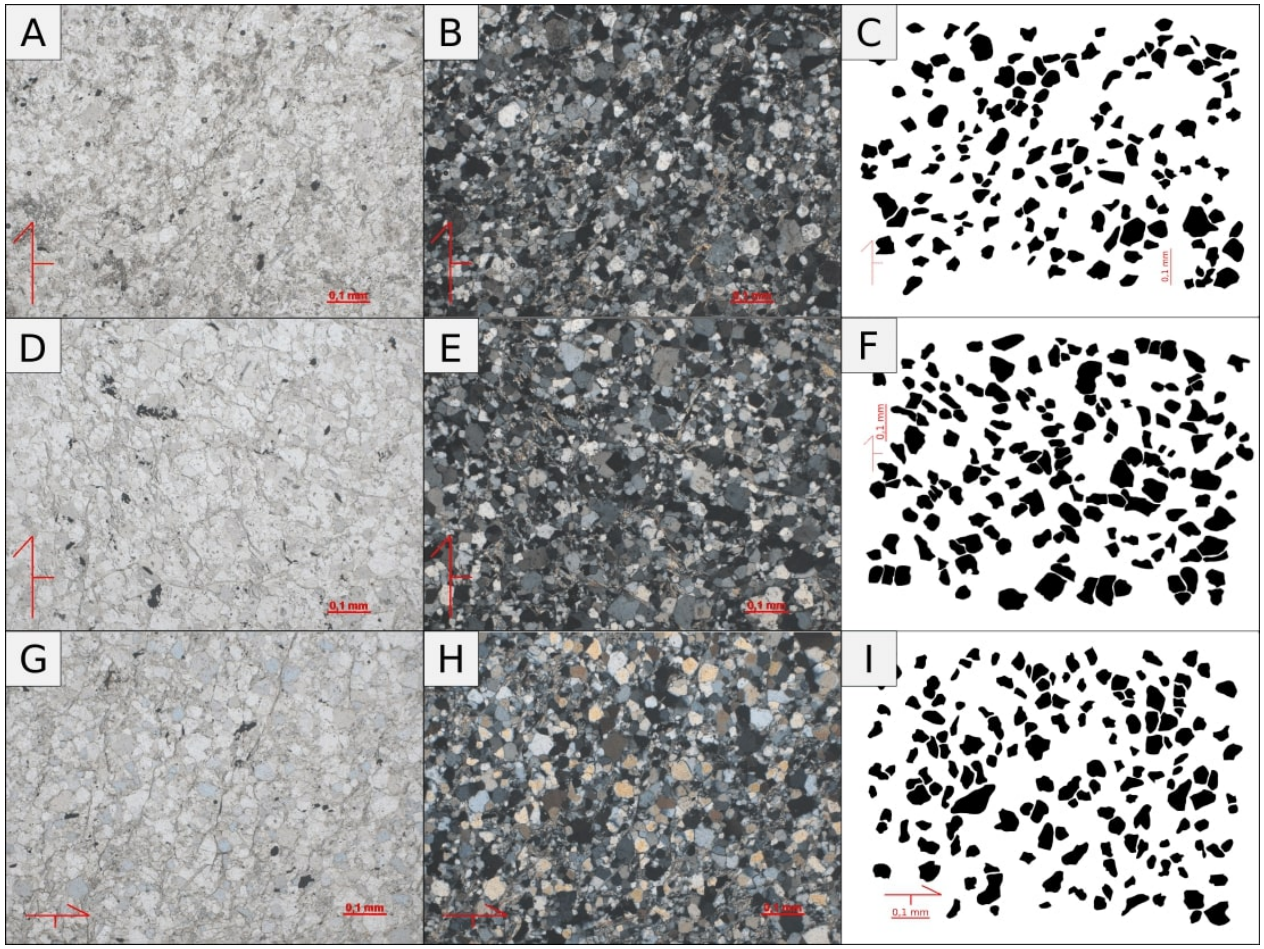

Figure 36: A,D,G: Polarized light microphotograph of the thin sections of planes AC, AB and BC of sample CD-40, respectively. **B, E, H:** Cross-Polarized light microphotograph of the thin sections of planes AC, AB and BC from sample CD-40, respectively. **C, F, I:** Single quartz grain digitized for SPO analysis of planes AC, AB and BC from sample CD-40.

The CD-40 sample is a well-sorted metarenite, with lepid-granoblastic texture, from the Serra da Gameleira Formation, interpreted as pre-rift phase sedimentation. This sample lies near a major thrust fault system, which thrusts the basement units on top of the sedimentary cover in a north-eastern direction. More than 500 grains of single quartz grains were analyzed, and all sections show low shape ratio values ranging from 1.11–1.14 (Figure 37). Thin sections microphotographs used to calculate the SPO are displayed in Fig. 36. The parameters of the best-fit ellipsoid can be seen in Fig.35.

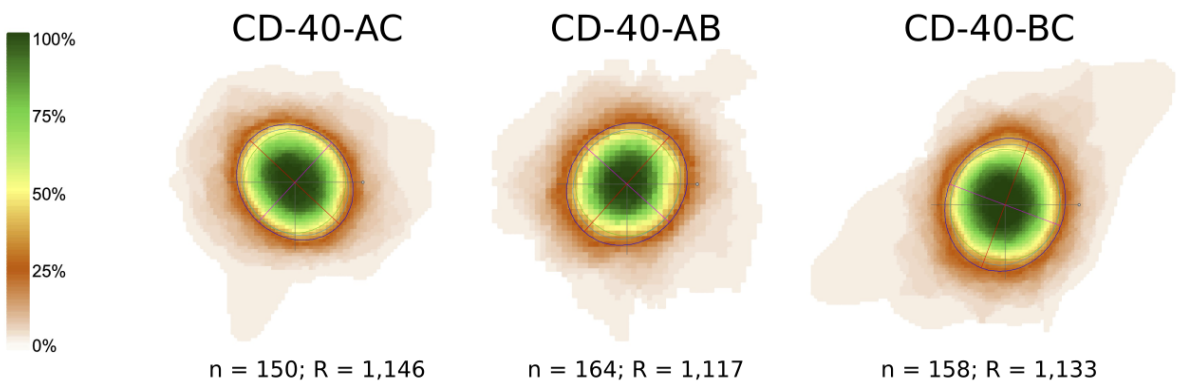

Figure 37: Shape preferred orientation ellipses from sample CD-40.

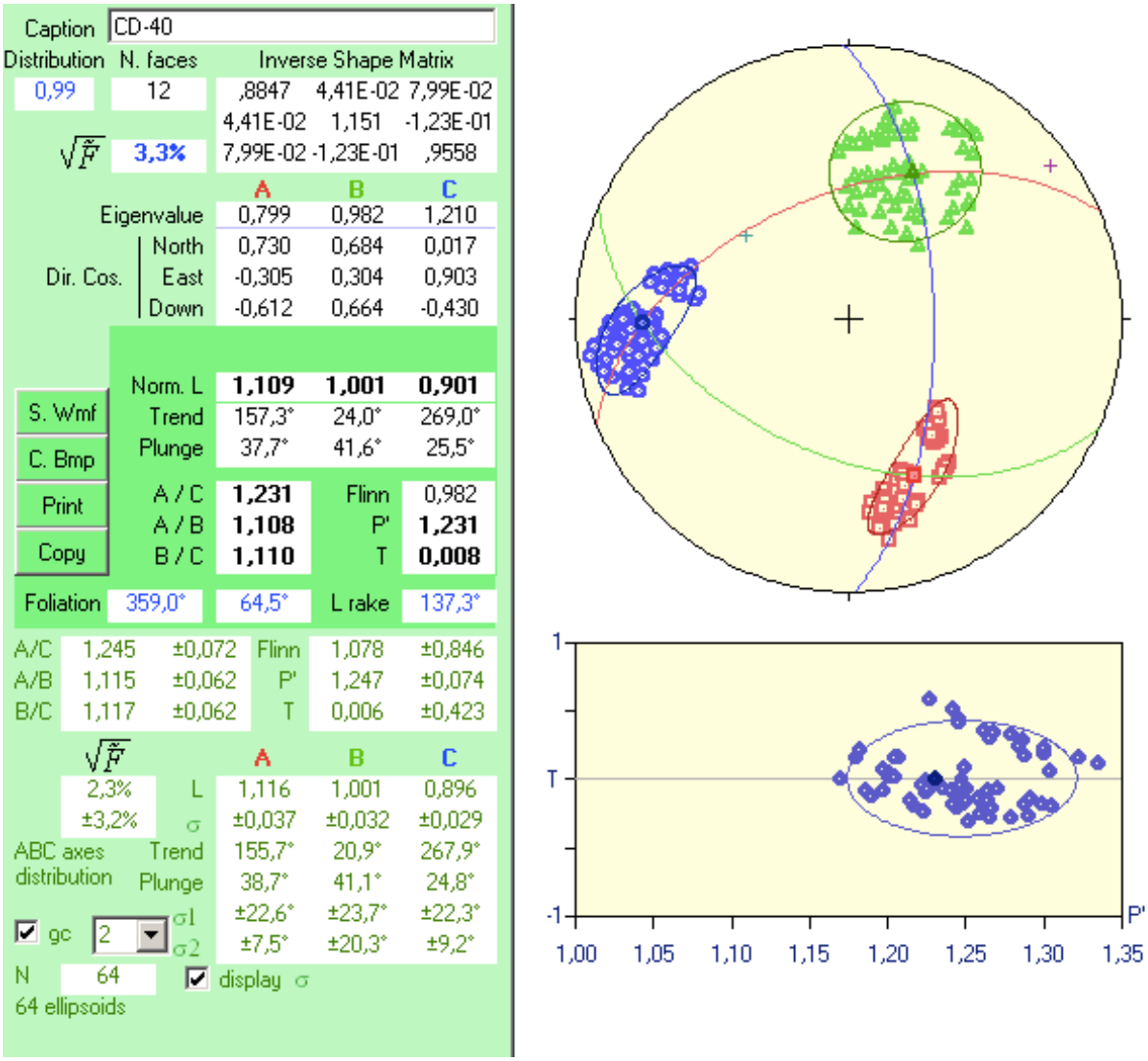

Figure 38: Best-fit ellipsoid parameters from Sample CD-40. Results direct from the program ELLIPSOID screen.